Analysis of Polybenzimidazole Feasibility in a Direct Methanol Fuel Cell Utilizing Temperature and Methanol Concentrations

A Major Qualifying Report
Submitted to the faculty of
Chemical Engineering Department
Worcester Polytechnic Institute
Worcester, MA 01609
May 1, 2014
By:

_____
Sean Callaghan

_____
William Lind

Approved by:

_____
Professor Ravindra Datta

Abstract

This report focuses on confirming the feasibility and on establishing the optimal operating conditions for a Direct Methanol Fuel Cell (DMFC) operated at high temperatures using a polybenzimidazole (PBI)-based membrane electrode assembly. PBI is known to operate well at high temperatures (160-180˚C), but its performance using methanol vapor instead of hydrogen bearing gas has yet to be characterized in detail. To this end, a PBI-MEA in an existing fuel cell apparatus was subjected to various conditions of operating temperature and methanol concentration. Tests were also conducted using an internal reforming layer on the anode side, which was comprised of an outer catalyst layer and gas diffusion layer contacting the anode. Results show that the performance of the cell increases with temperature up to about 240˚C at which point the PBI-MEA was damaged and showed reduced performance. The tests concerned with the effects of concentration showed that at higher temperatures there is only a small dependence on methanol concentration, and that at higher temperatures it is possible to operate at closed to the stoichiometric feed of methanol and water.

Executive Summery

The finite nature of fossil fuels and a new appreciation for the pollutants associated with their use has become of increasing concern of late. Because fossil fuels currently only produce energy by combustion, the conversion to electrical power is disappointingly inefficient. The fuel must be burned, and the thermal energy used to turn turbines and move generators, leading to large energy losses relative to the energy stored in the fuel to what can be extracted. Because of these inefficiencies, increased attention is being paid to devices which can extract useful energy from a fuel more efficiently and without such losses.

Fuel cells are seen as a viable alternative to produce electric power via burning fossil fuels because they are used to extract energy from a fuel and convert it directly to electrical current. One popular configuration for a fuel cell has a feed of hydrogen at the anode and a feed of oxygen or air at the cathode of the cell. When these gases are allowed to combine and react to form water in the fuel cell, the energy of that reaction can be harnessed as electricity. Cells using this reaction have existed for years and have been refined to the point where they can provide good efficiently and reliability of use. The problem with implementing a hydrogen fuel cell is in storing and feeding the hydrogen fuel itself. Hydrogen must be stored at high pressure to keep its volume to a manageable size, and if a leak occurs, great care must be taken considering hydrogen's high reactivity and the possibility of explosion. As an alternative, methanol can be used as the fuel in a Direct Methanol Fuel Cell (DMFC) because of its high power density and ability to be stored as a liquid. Some issues that arise when using methanol as a fuel are the possibility of methanol crossover from the anode to the cathode, where the methanol is reacted but without producing electricity and catalyst poisoning where the metal

catalyst used to enhance the reaction becomes fouled and performs with lower efficiency. Because of resulting slower electrode kinetics than for hydrogen, the catalyst loadings in DMFC tend to be much higher (by about one order of magnitude). Because the catalyst can be a precious metal like platinum, methods of achieving high performance with lower catalyst loading is of special concern.

The objective of this report is to present findings characterizing the performance of a DMFC under various conditions of temperature, fuel concentration and electrode configuration. This will provide an understanding to future investigators of what conditions are favorable and will help push research and development toward a more efficient DMFC setup by optimizing the operating conditions. To this end, we utilized a fuel cell using polybenzimidazole (PBI) as the proton-exchange membrane. This cell was tested at temperatures of 160, 170 and 180˚C, as this range is the one suggested by the manufacturer. When as expected, it was observed that the kinetics of the reaction and therefore the performance of the cell increased with temperature, the cell was further tested at 200, 220 and 240˚C to find the limit of the operating temperature before thermal damage to the cell. We also tested various concentrations of methanol fuel ranging from 3M to 24.7M (neat) methanol in water. Finally, the cell apparatus was modified to include a double-thickness anode layer to see if the additional catalyst contact would increase the performance of the cell via internal reforming.

These tests showed that the performance of the cell increases with temperature up to about 220˚C at which point components of the cell are damaged by the heat. When increasing the concentration of the fuel, better performance was observed at higher concentrations up to 10M until the cell was run using a feed of 17.1M methanol in water (a 1:1 molar ratio). Based

on this, it can be said that the optimal concentration of methanol is likely in the range between 10M and 17.1M. The cell was also operated using an internal reforming layer gas diffusion layer and catalyst layer to see what effect pre-reforming the fuel would have on the cell. At high temperature and feed concentration, the internal reforming layer is able to provide slightly improved performance over the stock membrane electrode assembly.

Acknowledgements

This project was collaboration between many individuals and built off of previous works.

First, we would like to thank Samatha Do, Kaitlyn Spetka and especially Matthew Suarez who started the research into high temperature direct methanol fuel cells using PBI that was the basis for our project. Matthew also aided us through showing us how to use the lab equipment and answer any questions about procedures that we had.

We would also like to thank Nick Deveau and Drew Martino for being the there in the lab when we needed them and putting up with us for hours at a time. They helped to guide us and looked after our tests when we were not able to even shutting it down once when the cell vented due to high pressure.

Finally, we would like to thank Professor Ravindra Datta for his guidance throughout our project and allowing us to continue the work in his laboratory. He was an indispensable source of understanding and aid whenever we were stuck or needed a push in the right direction.

Contents

Table of Figures

1. Introduction

According to the World Energy Outlook, the current global energy demand is on the order of 560 TJ (terra joules) in 2013 (International Energy Agency, 2013). Over the next decades, the demand is projected to increase to 730 TJ by 2035, underscoring the ever-increasing need to establish alternative energy programs. Of the energy produced currently, it is estimated that 66% is derived from burning fossil fuel, with the majority produced by burning coal or its derivatives (Institute for Energy Research, 2014). It has been known for decades that creating energy from burning hydrocarbon-based materials creates billions of tons of carbon dioxide gas worldwide and other greenhouse gases which contribute to global climate change; it is within this context that we explore the direct methanol fuel cell as a potential supplement to some of the current applications of hydrocarbon energy. Fuel cells are promising technologies in the effort to move away from fossil fuels because they have good efficiency, and can be assembled in a variety of sizes to fit many demand specifications (Ortiz-Rivera, et al., 2007). DMFC's may have potential applications for "light-traction vehicle applications" because of the high energy density of the fuel, the ability to easily replenish the fuel, and the relatively light weight of the cell (compared to an acid battery) (Kang, et al., 2012). Alternately, it may be used to recharge the battery on the run.

Though the principles of electrochemistry and electrolysis were known previously, the fuel cell is considered to have its inception in 1838 when William Grove harnessed the energy created in water formation to create an electrical current (Andujar, et al., 2009). Grove's "gas battery" functioned by combining hydrogen and oxygen gases, and transporting the resulting free electrons through a wire to facilitate the oxidation-reduction reaction. The reactions and

materials were updated in the following years, and now fuel cells serve to provide power to areas where an electrical grid is infeasible.

This report focuses on the use of methanol as a fuel in a fuel cell which was originally purposed for a feed of a hydrogen containing gas. This was done to investigate the feasibility of methanol as an alternative to the hydrogen, whose application is often logistically challenging. Hydrogen must be kept as a cryogenic liquid, and is therefore prone to leakage and has the potential to explode if handled improperly. Methanol has safety concerns of its own, namely its toxicity if handled directly, its high volatility and low flash point. The flammability of methanol can, for some arguments, be ignored, because all fuel alternatives like gasoline, diesel fuel, or hydrogen gas have the same issues. However, within the context of fuel cells, methanol has a significant advantage over hydrogen in that it is stored as a liquid and can be easily replaced (without the need for an operator to handle pressurized tanks).

Methanol is a very attractive liquid fuel for fuel cell-based power generation since it is inexpensive, widely available, and produced from environmentally attractive resources (natural gas). However, direct methanol fuel cells (DMFCs) suffer from poor performance despite very dilute feeds (1M) due to their high electrode polarization because of self-poisoning from carbon monoxide formed at the anode from methanol reforming, low durability of Pt/Ru catalyst needed for CO cleanup at the anode, low efficiency because of methanol crossover, and high cost due to high catalyst loading. This is compounded by the use of Nafion® membrane as electrolyte, which limits the operating temperature to less than 80°C, as it requires liquid water in its pores for proton conduction. Nonetheless, DMFCs are making significant inroads into small-scale portable applications.

The current state of the art in fuel cell technology utilizes specially fabricated materials to optimize the kinetics and process overall to achieve the best possible performance. As fuel gases are fed into the cell, they pass through specially designed serpentine channels intended to maximize the area of the catalyst which is exposed to the gas (Datta, 2014). Instead of using bulk platinum as in Grove's 1838 design, modern fuel cell use platinum nanoparticles to enhance the active surface area without the need for an excessively large apparatus (Modestov, et al., 2009) (O'Hayre, et al., 2009). To facilitate the transport of protons, specialty polymer electrolytes have been developed which hold acidic compounds and efficiently ferry the protons between electrodes.

In choosing materials of construction for a fuel cell Membrane Electrode Assembly (MEA), special attention must be paid to the choice of membrane which will transport protons across the apparatus. Two of the common choices are Polybenzimidazole, or PBI and Nafion® - 117 polymers (Gubler, et al., 2007). For the fuel cell used in this report, our predecessors chose to recommend a PBI membrane over Nafion®, for reasons of stability at higher temperatures. When using methanol as the fuel in the cell, PBI has been shown to tolerate higher concentrations of alcohol with around half of the methanol crossover seen in Nafion® at similar concentrations. Specifically, our fuel cell uses Celtec-P1000 Polybenzimidazole MEAs manufactured by BASF designed for a hydrogen gas feed. This product was selected for its high durability; it has been observed to operate for 20,000 hours at 160˚C with a feed of dry hydrogen and air.

The current-producing reaction occurring in the direct alcohol fuel cell is endothermic, and the harmful reaction of carbon monoxide absorption on to the catalyst is

exothermal; therefore the cell shows better kinetics at higher temperatures. The manufacturer of the membrane electrode assembly used in this fuel cell (BASF) advises that the cell be operated between 140 and 180˚C; however it logically follows that increasing the temperature beyond this limit will increase the performance of the cell up to the point where the heat damages the MEA itself or other components of the apparatus (Henschel, 2012). We decided to investigate this limit.The feed to such a fuel cell must be in the vapor form. If any liquid is present in the cell and contacts the MEA it can strip the phosphoric acid from the electrolyte layer which will come out of the cell into the channels crystalizing when the liquid evaporates. This leaves a powder buildup on the MEA which prevents the feed gases from contacting correctly and causes the pressure in the cell to increase to a point where it must be shut down. Another common mode of failure is that of catalyst degradation and crossover. When the cell is operated at high temperature for long periods of time, the metal can dissolve and migrate from the catalyst particles reducing the catalyst's effectiveness. Oswald ripening, in which catalyst nanoparticles agglomerate, reducing catalyst active area is another mechanism of fuel cell degradation. Fuel crossover also reduces the cell's ability to operate at the highest efficiency. In this case, the fuel methanol moves through the MEA reacting to produce a current. Instead of reacting at the anode where it is fed, the methanol can be diffusively transported to the cathode where it reacts directly with the oxygen feed. The amount of crossover observed increases with the operating temperature of the cell, but the detrimental effects are not of the same magnitude because of the increased kinetics.

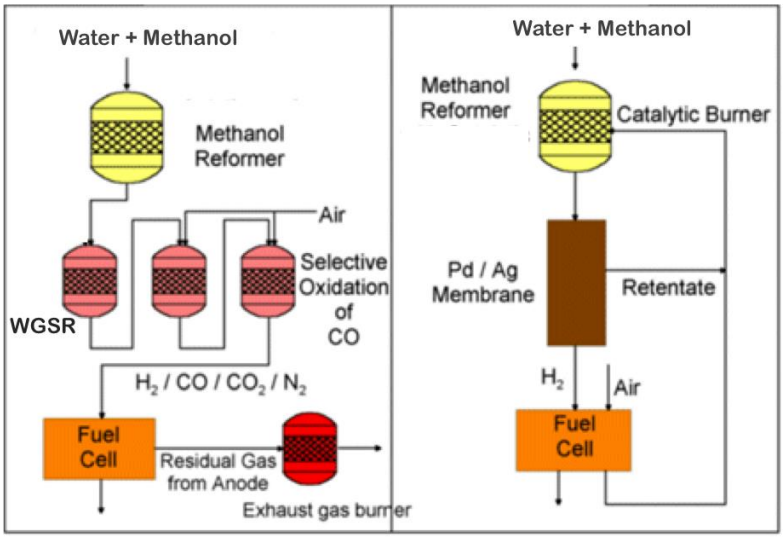

FIGURE 1: METHANOL REFORMER WITH WGSR AND PROX OR WITH PD/AG MEMBRANE (HTTP://WWW2.FZ-JUELICH.DE/).

For larger-scale portable or transportation applications, a reformer-PEM fuel cell combination appears more practical (Figure 1) (Wiese, et al., 1999). However, reformers are bulky because of the water-gas shift (WGS) and preferential-oxidation (PrOx) stages needed for the CO removal, besides a vaporizer, heat exchangers, and a catalytic burner, etc. Pd-membrane based integrated or separate (Figure 1) reformers are thus also being explored to reduce the complexity and bulk, but add to the cost (Israni, et al., 2011).

Here, we investigate a newer approach where we use methanol directly in a higher temperature fuel cell so as to allow higher feed concentrations, lower catalyst loading, and absence of Ru alloyed in the catalyst nanoparticles. Since Nafion© is limited in operating temperatures, we use PBI-phosphoric acid membrane-based MEA which is actually designed by BASF to operate from 160-180˚C for reformate gas in conjunction with a reformer (Figure 1). We show that performance rivaling room temperature conventional DMFC can be obtained especially at the higher operating temperatures (> 200˚C). Further, by using a reversed anode layer as an internal reforming layer, we investigate if enhanced performance can be achieved.

However, we find that increased diffusion resistance through double gas-diffusion electrode counters any effect of enhanced kinetics.

The purpose of this report is to determine the operating characteristics which exist in a high temperature direct methanol fuel cell. We report the findings on the effects of concentration changes in the feed, temperature changes of the cell, and of internal pre-reforming of the methanol fuel. It is known that increases in temperature will improve the kinetic rate of a reaction, so this report takes this concept to the extreme and tests the performance well above the recommended temperature to investigate the limit of the MEA before it is damaged by the heat (Fogler, 2005). Similarly, increasing the concentration of fuel (at a constant flowrate) was found to increase the performance of the fuel cell. It was unclear, however, if increasing the concentration of the fuel would result in a continued increase in performance or if there existed an optimal concentration. Finally, work has shown that partially reacting a fuel feed before it is allowed to meet an electro-catalyst layer can improve the performance of fuel cells by increasing the conversion of fuel to protons (Avgouroloulos, et al., 2012). To that end, we altered the apparatus setup to include an additional outward facing catalytic layer at the anode fuel inlet to allow the fuel to contact more reforming catalyst before reacting with the oxygen feed at the cathode. We expected this to produce an increase in the performance by allowing more of the alcohol fuel to react, producing higher current than in the stock apparatus makeup, and increasing the predictability of the readings by reducing variability in the conversion of methanol to water.

The following sections outline the historical development of the fuel cell and how the state of the art has developed from its origins. Once this is established, we will move to a

description of the methods used to test various aspects of the apparatus, and display the results seen following these tests. Finally, the results are contextualized and summarized, so that recommendations for future work on this apparatus can be made.

2. Background

This section presents a summary of the historical development of the electrochemical cell, and the continued development which has brought the technology to its present state. The mechanisms by which electricity is produced are covered, and the typical performance of a cell discussed to provide a fuller understanding for the results which follow.

History

Currently, about 66% of electricity generated in the United States is derived from of fossil fuels (Institute for Energy Research, 2014). Fuel cells are a viable supplement to burning fossil fuels because they can be operated at high efficiency, and are modular: able to be scaled to meet many size requirements. Unlike combustion of fossil fuels, fuel cells convert chemical energy directly into electrical energy, without the need to first produce thermal energy, leading to inefficiencies. Fuel cell technology is divided into categories based on the fuel used, the electrolyte used, and the method by which energy is extracted from the fuel. Proton Exchange Membrane, Molten Carbonate, Solid Oxide, Alkaline, Phosphoric Acid and DMFC are the main types of fuel cells currently in development and use around the world.

The history of the fuel cell begins in 1838 with William Grove's development of a constant-current cell using the combination of hydrogen and oxygen (Andujar, et al., 2009) (Ortiz-Rivera, et al., 2007). Grove used his knowledge of electrolysis and water decomposition to create a cell (Figure 2: Schematic of the Grove Gas Battery) which consisted of two platinum electrodes; one end of both was immersed in sulfuric acid, and the other end of one in hydrogen, and oxygen. When the electrodes were connected by an eternal circuit, Grove

observed a constant current generated from the combination of hydrogen and oxygen into water. Grove connected several of these cells in series and observed an increase in the potential drop across the electrodes. This apparatus, which Grove referred to as a “gas battery” is considered to be the first fuel cell. Figure 2 shows the apparatus Grove used in his experiments (Smithsonian Institution, 2004). The right-most section of the apparatus is a voltmeter, wherein the volume of gas indicates the amount of oxygen (in the tube labeled “o”) or hydrogen (in the tube labeled “h”) in the system.

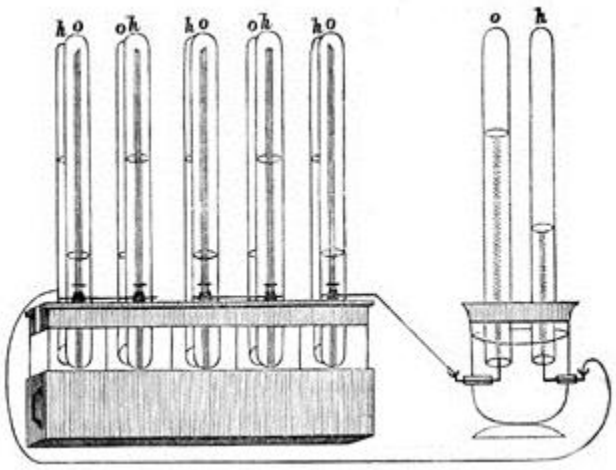

FIGURE 2: SCHEMATIC OF THE GROVE GAS BATTERY

The understanding of the mechanics of fuel cells came in 1893 with Friedrich Oswald’s work connecting the functions of the electrodes, electrolyte, oxidizing/reducing agents, cations and anions. Oswald is considered the father of the study of chemical kinetics, and to this point, Grove was only able to speculate on the mechanism that allowed the fuel cell able to produce a current. Fuel cell technology took another quantum step when Mond and Langer successfully used coal as a fuel; this was the first time a substance other than elemental hydrogen was used,

despite Grove's belief that only hydrogen was capable of sustaining the operation of a fuel cell (Andujar, et al., 2009).

Francis Thomas Bacon worked to develop some of the most practical early fuel cells. In 1939 he devised a nickel gauze electrode alkaline fuel cell which operated at about 300 psi of pressure (Ortiz-Rivera, et al., 2007). During World War II, he developed fuel cells for the Royal Navy which were put into practical use in British submarines. Bacon's work provided such reliable fuel cell techniques that his work was eventually acquired by Pratt & Whitney Aircraft for use on the Apollo spacecraft.

In 1955, Thomas Grubb modified the original fuel cell specifications and used a membrane made of polystyrene as the electrolyte. This was followed in 1958 when Leonard Neidrach deposited platinum on the membrane to catalyze the hydrogen-oxygen reaction, speeding up the kinetics in the fuel cell. In the decades to follow, advancements were made which lowered the mass transfer resistance in electrodes and allowed for lessened diffusion limitations. This advancement, combined with the lower cost of catalytic materials and increased working lifespan improved the practicality of the fuel cell to levels which were previously unreachable.

Today, fuel cells have found application in areas where fossil fuel-based power generation is not appropriate. Because fuel cells are scalable, and do not produce environmental contaminants like gasoline generators, they have been used in hospitals and shelters where they can be deployed at the site of need without the need for an electrical grid (Andujar, et al., 2009). Fuel cells are also useful in locations where an electrical grid doesn't

exist. For example, the International Space Station uses a stack of hydrogen fuel cells to provide power when the station's solar array is inoperable (i.e. at "night") (Hadfield, 2014).

Rationale for Fuel Cell Use

There are several advantages to using fuel cells over conventional fossil fuel power plants that are being used and developed today. At present, majority of the market utilizes unrenewable fossil fuels. Emissions from these sources are also harmful to the atmosphere as well as damaging to the individuals and creatures that have to breathe in the contaminated air. Solar energy is much cleaner than that based on the combustion of fossil fuels but requires sunlight to operate efficiently and batteries to store electricity and operate when direct sunlight is not available. Batteries are also used in conjunction with wind, nuclear and other "cleaner" energy sources, but are large and require the use of metals which after long term use turn into waste. These issues however can be overcome by the use of fuel cells. Unlike batteries that store electricity, fuel cells use no metals but rather produce power so long as supply of a fuel continues. Additionally the waste of a hydrogen or methanol fuel cell is mostly water, CO_2, and little of other pollutants such as SO_2 and NO_x. Fuel cells also allow for the transportation of the energy source in the form of hydrogen or methanol which can be easily stockpiled and renewed unlike a battery whose limit, once reached, cannot be exceeded. This means that fuel cells have the potential to operate with the convenience and reliability of gasoline while also utilizing a potentially renewable resource with a smaller environmental footprint.

Introduction to a Typical Fuel Cell

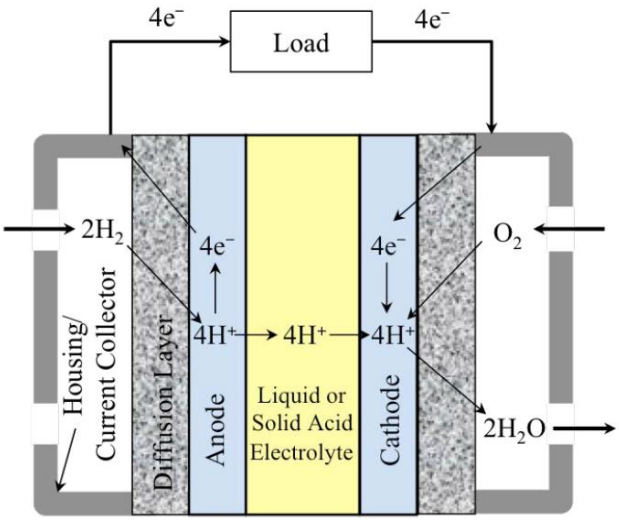

FIGURE 3: CUT-AWAY SCHEMATIC OF A FUEL CELL (DATTA, FUEL CELL BASICS, 2014, PG. 54). NOTE THAT THE APPARATUS USED IN THIS REPORT UTILIZES A FEED OF ALCOHOL WHICH IS CATALYTICALLY REFORMED INTO HYDROGEN.

The basis of fuel cell operation (Figure 3) is a reduction/oxidation set of reactions that produce and consume electrons which is allowed to take place in the cell at different electrodes, converting the fuel materials into product species. As these reactions proceed, electrons and ions are separated from each other, creating a potential differential across electrodes in the cell. The hydrogen-oxygen fuel cell operates by a catalytic reaction of a hydrogen feed to produce protons and electrons and the subsequent reaction with oxygen to form water. When the hydrogen first enters the anode side of the cell, it contacts a metal catalyst (in some cases platinum alloyed with other metals) which causes the hydrogen to dissociate into protons and electrons. These free protons are transported through a polymer electrolyte material as they cross the cell to the cathode side. In this step, ideally only protons are transferred between the electrodes, as crossover of intact fuel species causes reduced

performance (crossover is discussed in more detail later). This reaction is very thermodynamically favorable, and will proceed nearly to completion, especially at the elevated temperatures at which some fuel cells operate. The conversion of elemental oxygen and protons to water requires the oxygen to be reduced, a process which can only happen in the presence of catalyst and of the free electrons which were created at the anode. When these reactions have established themselves, and an external circuit is completed between the two electrodes, the electrons freed in the oxidation reaction will flow through the circuit and arrive depleted of some of their energy to facilitate the completion of the reduction reaction. Current and power are generated from a fuel cell when useful work is done with the flow of electrons before they are allowed to participate in the reaction mechanisms.

Components of a Fuel Cell

Electrode Catalyst

In general, the purpose of the catalyst layer is to provide a surface that can facilitate the dissociation of the species necessary for the energy-producing electron-exchange reactions in the cell. Sites on the catalyst surface serve as intermediate bonding points for species dissociated from their original species. Protons are transported through a semipermeable electrolyte layer to cathode catalyst layer where they react with oxygen from a gaseous feed. In the Membrane Electrode Assembly, the catalyst is coated on to the gas diffusion layer. The catalyst is necessary because the polymer layer is only capable of transporting protons through the layer; it is not capable of producing protons from a chemical species such as H2. As the protons are reacted with oxygen on the cathode catalyst to form water, electrons released in

the dissociation of H2 are allowed to travel through an external circuit to join the reduction-oxidation reaction taking place at the cathode. The specific mechanism by which the protons are produced from hydrogen has been theorized to take place in three mechanistic steps, where protons exist as hydronium ions (Ohtake, et al., 2007) (Datta, 2014):

(1) HEYROVSKI: $\mathbf{H_2 + H_2O + S \rightarrow H - S + H_3O^+ + e^-}$

(2) VOLMER: $\mathbf{H - S + H_2O \rightarrow H_3O^+ + e^- + S}$

(3) TAFEL: $\mathbf{H_2 + 2S \rightarrow 2H - S}$

Platinum is used as the catalyst to facilitate both electrode reactions because of its ability to dissociate chemical compounds on its bonding sites and produce ions, which can be used to create a potential differential across the cell, producing power when a circuit is completed (Barczuk, et al., 2010). Metal catalysts typically take the form of nanoparticles of metals or alloys supported on carbon particles, which allows for very high active surface area without need for a large apparatus (Datta, 2014). Using nanoparticles of catalyst, hence, active areas of 100-200 cm^2 active area per cm^2 of MEA area can be expected, greatly increasing the amount of sites over the use of, e.g., metal foil. O'Hayre (2009) states that platinum nanoparticles have an optimal size of 2-3 nanometers (O'Hayre, et al., 2009).

Pure platinum is also known to have a high affinity for bonding to CO, however, which can cause loss of efficiency when bonding sites are occupied with CO and can therefore not be used to dissociate hydrogen. Because of this, effort has been put into alloying the platinum surface with different metal atoms. Thus platinum/ruthenium alloys are employed because they can aid in the removal of adsorbed CO and other intermediates (Kang, et al., 2012) with the help of dissociated water. Ruthenium is used because water can be activated (at lower over

potential than on Pt) to react with the CO adsorbed to adjacent Pt atoms by the mechanism (Datta, 2014):

$$\mathbf{2H_2O + S \rightarrow HO - S + H_3O^+ + e^-} \quad \textbf{(4)}$$

$$\mathbf{CO - S + OH - S + H_2O \rightarrow CO_2 + H_3O^+ + e^- + 2S} \quad \textbf{(5)}$$

Where S represents an open catalytic bonding site, and R-S represents a species R adsorbed to a bonding site. The end product of this reaction, CO_2 can then exit the apparatus, clearing bonding sites on the catalyst for current producing reactions. This reaction is more favorable with a large overpotential driving force, which can result from the buildup of CO itself. This leads to a self-sustaining cycle in which CO builds up on the catalyst surface, reducing the operability of the anode electrode and increasing the overpotential. When the potential reaches a high enough point, the above reactions will take place, clearing the catalyst and dropping the potential differential of the cell. When this condition is met, the clearing reactions no longer take place and CO builds up on the catalyst, restarting the cycle. This leads to an oscillation of the cell voltage, which reaches its lowest point right before the clearing reaction takes place, and its highest point immediately after water activation has moved CO off of the catalyst surface.

Because the adsorption of CO to the catalyst layer is exothermic in nature, operating a PEM fuel cell at high temperature also cuts down on CO poisoning. At 80˚C, a fuel cell can be expected to tolerate about 10 ppm CO in a hydrogen feed without substantial losses. If the operating temperature is increased to 150-200˚C, however, CO impurities of up to 1% in the hydrogen feed can be tolerated. However, Nafion works only when it has liquid water in its

pores through which diffusion of protons occurs. Consequently PEM fuel cells are limited to an operating temperature below 100˚C.

Over the life of a membrane electrode assembly, the catalyst will undergo degradation whereby the size of the metal nanoparticles increases and the surface area decreases, slowing reaction kinetics (Kang, et al., 2012); (Modestov, et al., 2009). This sintering of particles is known as Oswald Ripening, and occurs when thermal forces cause agglomeration of nanoparticles into large particles, which are more thermodynamically stable with a smaller surface area per unit volume. Through lifetime tests of MEAs, it has been established that the total platinum concentration in the catalyst layer remains unchanged, leading to the conclusion that the loss of kinetic activity is due to a loss of surface area with the existing metal (Modestov, et al., 2009).

Alloying platinum with other metal atoms has also shown promise in improving reaction kinetics over the use of pure platinum. Alloys improve the oxygen reduction reaction by shortening the distance between adsorbed species and their nearest neighbor (Colon-Mercado, et al., 2006), and by reducing mass-transport loss associated with clearing water from the catalyst (Wang, et al., 2010). Colon-Mercado & Popov (2006) have presented work showing that some alloys of platinum actually have lower surface area than pure platinum, but that alloys' surface area will not decline as rapidly as pure platinum giving them a longer life overall. This is associated with an anchoring effect wherein the alloying metal shows added affinity for the carbon support material, thus reducing Oswald ripening.

It has been proposed that electrocatalysis could be enhanced with heteropolyacids such as phosphododecamolybdic adic ($H_3PMo_{12}0_{40}$) to increase conduction of protons produced

(Barczuk, et al., 2010). The rationale is that thin films of these acids would serve to activate the catalytic nanoparticles, thus also preventing agglomeration without blocking Pt active cites themselves. Barczuk (2010) found that pure platinum, as well as Pt-Ru and Pt-Sn alloy supported on Vulcan carbon support all showed improved current performance with the addition of phosphododecamolybdic acid.

Anode Reaction

The current-producing reaction which takes place at the anode, is the dissociation of elemental hydrogen into individual free protons. These protons are subsequently transported through the cell and are allowed to react at the cathode, creating the potential differential in the cell.

$$\mathbf{(6)} \qquad \mathbf{H_2 \rightarrow 2H^+ + 2e^-}$$

The chemical equation taking place at the anode is described above as Equation 6 (Datta, 2014). When hydrogen fuel is added to a fuel cell apparatus, it is fed to the anode electrode side of the device. The fuel contacts the catalytic layer where protons can be stripped from the fuel and water on catalyst sites. Once dissociated, the protons are free to move through the polymer electrolyte layer by the Gotthuss and Vehicle mechanisms (described below) to arrive at the cathode electrode. As this progresses, if stable intermediates such as CO are produced from the fuel, they can foul the sites of the catalyst, causing significant reduction in energy output (Datta, 2014). As protons move across the electrolyte layer to the cathode, a potential differential develops, since the electrons are liberated in the anode reaction, but are not allowed to travel with the protons to the cathode. The use of an external circuit allows the

electrons to move from the anode to the cathode to reconnect with the protons, thus promoting the cathode reaction and producing usable electrical energy from the cell apparatus and releasing the balance as waste heat.

Cathode Reaction

The idealized oxygen reduction reaction which takes place at the cathode electrode of the fuel cell is:

$$(7) \qquad O_2 + 4H^+ + 4e^- \rightarrow 2H_2O$$

which is used by the cell to produce a current (Kamarudin, et al., 2013) (Kim, et al., 2011) (Park, et al., 2012) of the standard reduction potential for this reaction is 1.229 Volts (Datta, 2014) (Miessler, et al., 2011). The hydrogen atoms are transported through the polymer layer to the cathode, where this reaction occurs. For the reaction to take place however, electrons must also be present. The cell produces energy by only allowing the electrons to move from the anode to the cathode by passing through an external circuit and doing useful work for the user (Datta, 2014).

Nafion®

One common polymer electrolyte membrane (PEM) used in conventional hydrogen fuel cells is Nafion®, which is based on a tetrafluoroethylene backbone, and contains covalently attached sulfonic acid side chains (DuPont Fuel Cells, 2009) as shown in Figure 4. This polymer is employed because of its ability to transport free protons from the anode catalyst layer to the cathode in the presence of water, where they can react with an oxygen feed to produce a chemical reaction and an electrical current. The transport of protons is achieved by using the

acidic side chains of Nafion to dissociate into hydronium ions in the presence of water, and transport them via the Grotthuss as well as the Vehicle mechanisms (Datta, 2014).

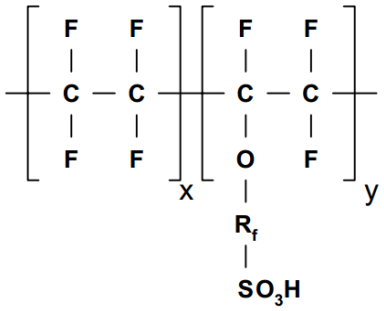

FIGURE 4: BASIC MONOMER STRUCTURE OF NAFION®, ADAPTED FROM (DUPONT FUEL CELLS, 2009)

In the Grotthuss Mechanism of transport Figure 5, stationary proton acceptor/donor vehicles (in this case water molecules) "pass" charged particles from one site to the next, accepting a charge imbalance from an adjacent species, only to subsequently lose the charge balance by propagating the motion of the charged particle (Agmon, 1995). It is also theorized that the motion of charged particles additionally occurs by the Vehicle Mechanism (Datta, 2014), shown schematically in Figure 6. By this mechanism, a hydronium ion would be formed to take on a charge, and through a voltaic driving force, would be moved from one position to another, thus transporting the particle along with it. When the ion finds a thermodynamically stable place to "put down" the particle, it will be relieved of its charge, and will move by diffusion to its original location to take up another charge and begin the process again.

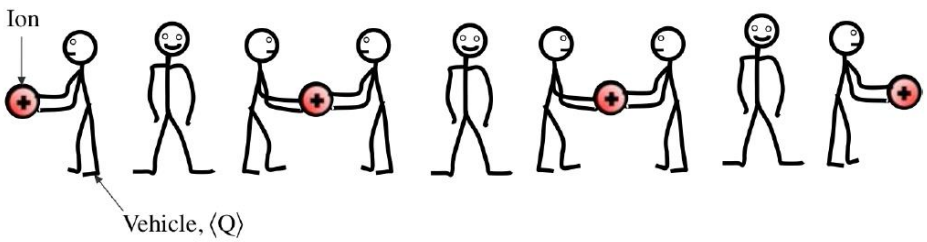

FIGURE 5: SCHEMATIC REPRESENTATION OF GROTTHUSS MECHANISM OF ION TRANSPORT (DATTA, 2014) ADAPTED FROM (KREUER, ET AL., 1982).

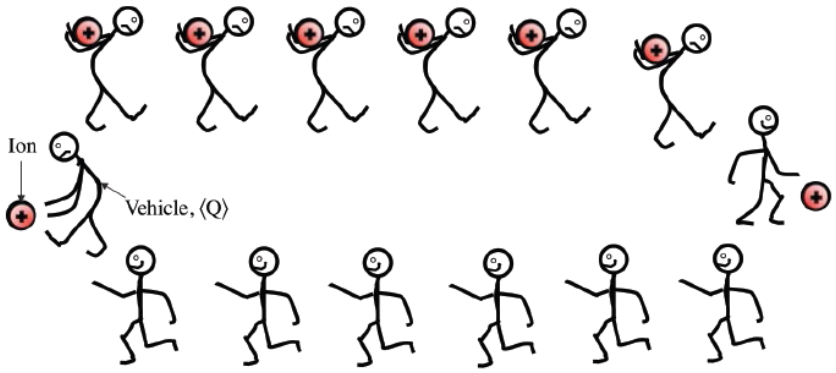

FIGURE 6: SCHEMATIC REPRESENTATION OF THE VEHICLE MECHANISM OF ION TRANSPORT (DATTA, 2014) ADAPTED FROM (KREUER, ET AL., 1982).

Performance Issues

The voltage provided by a fuel cell is given by:

$$\mathbf{V} = \left(\Phi_{C,0} - \Phi_{A,0}\right) - \left(\eta_{A,k} + \eta_{A,D} + \eta_{A,x}\right) + \left(\eta_{C,k} + \eta_{C,D} + \eta_{C,x}\right) - \eta_{EL} - \eta_{I} \quad (8)$$

This equation 8 describes the various factors which prevent the cell from realizing its full theoretical voltage. The theoretical maximum or Nernst potential is defined simply as the

difference in potential between the cathode and anode (represented by the first term above). The second and third terms above represent the potential losses in the anode and cathode (respectively) because of the kinetics of the reduction/oxidation reaction (ηk), and diffusional motion of species (ηd) as well as losses associated with fuel crossover between electrodes (ηx). Real-world performance is also influenced by the Ohmic potential drop associated with electrolyte layer ion conduction (ηEL), and potential drop from any interfacial resistance (ηI), though this is negligible in most cases. Though Ohmic resistance in a circuit is constant, the resistances described here are nonlinear and each vary as functions of current density of the cell. The additive reduction of all potential losses described above accounts for the nonlinear voltage relationship in a polarization curve. The relative magnitudes of each of the overpotentials as functions of current density can be seen graphically in Figure 7, where the white space between the axis and the addition of over potentials represents the voltage observed in the cell as a function of current density.

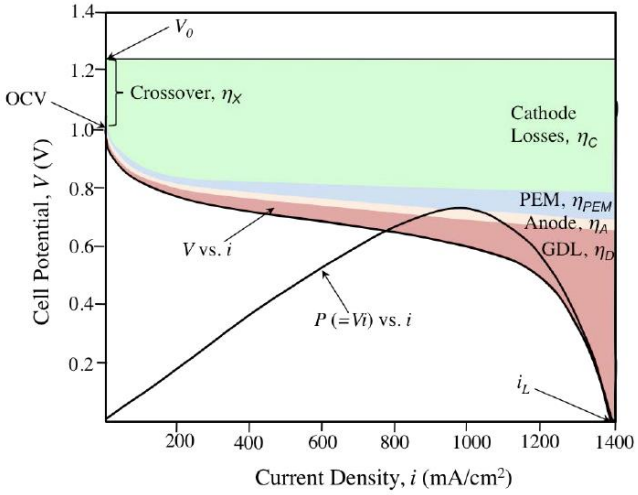

FIGURE 7: PLOT OF RELATIVE MAGNITUDES OF CELL OVER POTENTIALS AS FUNCTIONS OF CURRENT (DATTA, 2014).

At higher current densities, the slope of the curve will be dominated by resistance of the polymer membrane layer, with a linear Ohm's law dependence (Datta, 2014). At still higher current densities, however, potential will also be influenced by increasingly prominent mass transfer limitations of O_2 diffusion through the Gas Diffusion Layer (GDL) and catalyst layer.

As described above, the fouling of the catalyst layer by CO if present and subsequent clearance by ruthenium atoms causes a voltage cycle to build-up and clearance to occur at the catalyst surface. When this occurs in a cell, a cycling of voltage will be observed with low potential observed as fouling increases in magnitude, and a return to higher potential differentials when over potential become high enough to induce clearance (Datta, 2014). When a cell is run for extended periods of time under less-than-ideal conditions, this cycle of fouling will manifest as an observed oscillation of voltage with time.

At higher operating temperatures, it is observed that higher rates of kinetics contribute to higher overall performance, but higher diffusivity in the membrane layer also causes an increase in fuel crossover from the anode to the cathode (Pivovar, et al., 2003). This can be seen in a metric of the cell known as OCV or Open Circuit Voltage (alternatively Open Current Voltage) where the cell is operated with no external current to observe what potential the cell is capable of producing. As seem from equation 8 even at zero current the crossover overpotentials contribute to a voltage, OCV, less than the thermodynamic or Nernst cell potential. At higher temperatures, the observed OCV is typically lower than at more moderate temperatures, indicating that the over potential of crossover, η_x, is dependent on the temperature.

Feasibility of Hydrogen Fuel Cell

Currently the main form of fuel cell in use is the hydrogen PEM fuel cell. Researched over many years, it has become the standard within the fuel cell community to measure up against. Hydrogen fuel cells offer excellent performance when compared to methanol and other competitor fuels so far in research labs but that doesn't mean it is perfect. Many issues arise when looking into hydrogen as a standard fuel as opposed to that of methanol. The two largest of these are transportation and storage. Transportation of hydrogen over long distances is not economically feasible requiring the need for hydrogen production facilities every 50-100 miles. Over large regions, transportation would be similar to that of compressed natural gas, usually utilizing pipelines, as shipping via truck is not economically feasible with the relatively small load it could carry. Storage in vehicles is achieved via either cryogenic tanks or compressed hydrogen tanks. This is dangerous as a rupture could lead to an explosive result through a quick decompression of the tanks. When compared to gasoline, hydrogen's volumetric energy density is rather low at over three times lower than methanol and 3,000 at room temperature. This is significantly lowered to only half as much as methanol and about 3.5 fold lower than gasoline when in liquid form. (XCellsis, 2001)

Conventional Methanol Fuel Cells

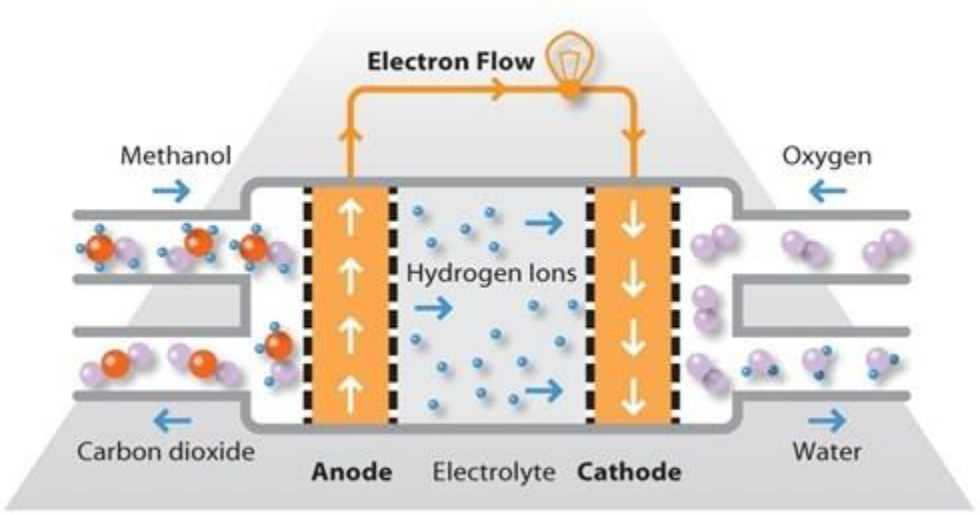

FIGURE 8: SCHEMATIC OF A DIRECT METHANOL FUEL CELL

(HTTP://WWW.YNOVEX.COM/IMAGES/DIRECT_METHANOL_FUEL_CELL.JPG)

Methanol as a Fuel

Methanol has seen commercial production for centuries, beginning with simple wood distillation and moving to more advanced methods of creating synthetic alcohol. The traditional route for producing methanol was simple wood distillation, leading to methanol's colloquial name "wood alcohol" (Tijm, et al., 2001). In 1923 the Badische Anilin- und Soda-Fabrik company (BASF) developed a method for producing synthetic methanol at high pressure. The new method required pressure of 250-350 bar and temperature of 320-450˚C, and was therefore a technical breakthrough. It was the development of a copper catalyst by Imperial Chemical Industries, however, that allowed the mass production of synthetic methanol, as the catalyst required much lower pressure of 35-55 bar and temperature of 200-300˚C. In the last 20 years, there have been improvements in of production technology proposed which may cause the

cost of bulk methanol to drop further, availability to increase, and the alcohol to become an even better fuel candidate. Fuel cells using alcohols in general are appealing based on their low fuel cost and ready availability (Kamarudin, et al., 2013). Thermodynamically speaking, methanol has a theoretical power density of over 6 kWh/kg (Kamarudin, et al., 2013); (Pivovar, et al., 2003). Giner Inc., a commercial distributor of fuel cell technologies claims that with their products, a fuel cell can expect to output about 1 kWh per liter of methanol used (Giner, 2014). Methanol is seen as a good candidate for fuel cells and energy applications in general, because it is easily stored in its liquid form (Zurowski, et al., 2010).

In the case of a liquid fuel like methanol, the fuel can be heated and vaporized before being fed into the anode of the cell, although in most cases it is fed as a liquid. In this reaction, the carbon atoms in methanol are oxidized to form CO_2 and protons and electrons are liberated. Once separated, the proton is allowed to travel through a Proton Exchange Membrane (PEM) to arrive at the cathode where it is recombined with an oxygen feed to produce water.

$$\mathbf{CH_3OH + H_2O \rightarrow 6H^+ + 6e^- + CO_2} \quad (9)$$

$$\mathbf{O_2 + 4H^+ + 4e^- \rightarrow 2H_2O} \quad (10)$$

$$\mathbf{CH_3OH + \frac{3}{2}O_2 \rightarrow CO_2 + 2H_2O} \quad (11)$$

It should be noted that, while Ohtake (2007) proposes that methyl formate is an intermediate product of the initial methanol reaction, others have proposed the presence of acetic acid (Zurowski, et al., 2010), though in either case, the predictable operability of the cell shows that free protons are produced and can proceed via participation of the other mechanistic steps as shown in Figure 9.

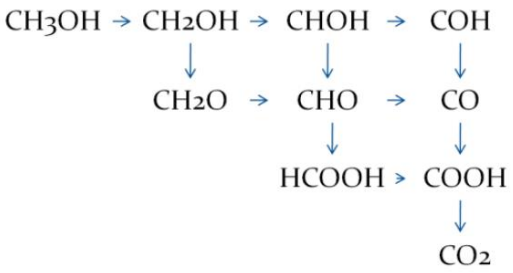

FIGURE 9: FLOWCHART OF MECHANISTIC STEPS BY WHICH METHANOL IS CONVERTED TO CARBON DIOXIDE THROUGH SEVERAL POSSIBLE STEPS (DO, ET AL., 2012)

As can be seen in Figure 9, the dehydrogenation of methanol to the final product carbon dioxide has many intermediates of varying stability. Of special concern is the intermediate carbon monoxide, as there are many mechanistic steps leading to the presence of CO, and it is known to cause fouling in the catalyst layer (Kang, et al., 2012). In a similar fashion to that used in a hydrogen fuel cell, the catalyst in a direct methanol fuel cell apparatus can be alloyed with different metals to aid in the removal of CO from the catalyst and prevent premature fouling. Equation 4 and equation 5, which describe the mechanism by which CO is cleared from catalytic sites, are also valid in the context of a DMFC.

The benefits of methanol as a fuel are that it is easily oxidized using metal catalysts, especially compared to more complex alcohols like ethanol (Zurowski, et al., 2010). Ethanol requires higher activation energy for oxidation because of the difficulty in breaking its carbon-carbon bond, a problem that doesn't exist in methanol. On the other hand, ethanol can be easily produced from biomass, and is far less toxic than methanol. Certainly a trade-off must be made between the energy efficiency of a cell, and the potential hazards associated with transporting and replacing the fuel.

Nafion® -based Methanol Fuel Cell

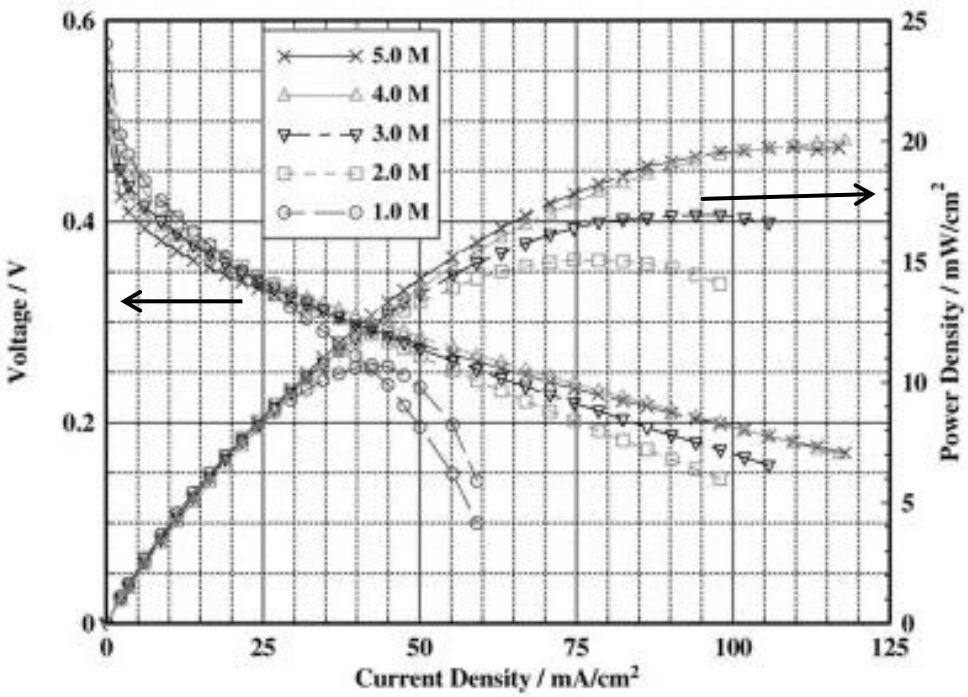

FIGURE 10. TYPICAL POLARIZATION CURVE FOR A PASSIVE DMFC USING NAFION® AT VARYING METHANOL CONCENTRATIONS. VOLTAGE AND POWER DENSITY ARE COMPARED TO CURRENT DENSITY OF THE CELL. ADAPTED FROM (LIU, ET AL., 2005)

The performance of a fuel cell is usually described by a polarization curve, such as Figure 10 which plots the voltage developed across the DMFC as a function of the current density of the membrane electrode assembly. This plot is developed by adjusting either the amperage or voltage in the cell (through the use of a load box) and recording the response of the other parameter. The current the cell produces is typically normalized as the current density which is the amperes in the cell per square centimeter of membrane electrode assembly. The current density is also graphed along with the power density of the cell. This term is defined by

multiplying the current density by the voltage of the cell, and has units of mW/cm^2. By defining current density and power density, performance of units of different sizes can be compared, assuming that both will be able to create about equal performance per active area. Figure 10 shows the performance of a passive direct methanol fuel cell using Nafion®, and operating under different concentrations of methanol. As can be observed in Figure 10, the peak power density for this setup was approximately 20 mW/cm^2, and the best performance results from dilute feeds. The apparatus used in preparing this report differs from that used for the above graph in that this apparatus is not passive; oxygen is fed in from a pressurized tank, not drawn from the atmosphere.

Catalyst Loading

In the direct methanol fuel cell as in the hydrogen cell, the purpose of the catalyst is to facilitate the dissociation of protons from the fuel so they can be transported from the anode to the cathode to react. The reactions which take place at the catalytic sites in a methanol fuel cell (Figure 9) are significantly more involved than those in a hydrogen fuel cell because of the increased complexity of the alcohol molecule compared to the elemental hydrogen diatomic molecule (Do, et al., 2012). Because of the slow kinetics of methanol oxidation and self-poisoning by CO, the catalyst loading is typically about ten times higher on a DMFC as compared to a H_2-O_2 fuel cell (Datta, 2014). A typical range for the catalyst loading in a conventional hydrogen fuel cell is about 0.4 mg/cm^2 for both the anode and cathode electrode sides of the MEA, whereas a DMFC is more likely to have a loading of around 4 mg/cm^2.

The anode reaction as described above in Equation 6 has been shown to have somewhat slower kinetics than the cathode reaction, so it is beneficial to a membrane electrode assembly to have a higher catalyst loading on the anode than the cathode (Cho, et al., 2008) (Datta, 2014). This is the case in the MEA used in preparing this report. The Celtec-P1000 MEA used contains a catalyst loading of 0.7 mg of platinum/nickel alloy on the cathode, compared to 1 mg of platinum black on the anode, designed to address this issue (Henschel, 2014), although the Celtec-P1000 MEA is designed for reforming hydrogen containing CO_2 and some CO.

Significant work has been done in improving kinetics at the anode by adding ruthenium along with the platinum particles in conventional DMFCs, though this has been shown to also create ruthenium crossover (Liu, et al., 2009). Throughout the working life of a cell using Pt/Ru catalyst layers, ruthenium can dissociate from the platinum particles of the catalyst and travel to the cathode, reducing the performance and efficiency of the system. Liang (Liang, et al., 2008)has proposed that adding gold particles can reduce ruthenium crossover as well as reduce CO build up on the catalyst. Similarly, Nandanwar has shown that the addition of polyvinylpyrrolidone (PVP), cobalt, rhodium or silver can reduce crossover when added to a catalyst layer (Nandanwar, et al., 2011).

Crossover

One of the major limitations on the performance of fuel cells is the effect of crossover, in which species fed to the cell migrate through the cell to react at the opposite electrode, thus preventing the cell from using that fuel for useful work (Park, et al., 2012) (Gubler, et al., 2007).

$$(12) \qquad CH_3OH + \frac{3}{2}O_2 \rightarrow CO_2 + 2H_2O$$

This equation 12 describes the reaction which takes place when methanol and oxygen contact directly, as is the case in species crossover. This reaction equation is identical to the overall reaction of the fuel cell, but when this reaction takes place at the cathode with methanol which has crossed over to react with the air feed, it cannot create electricity (Datta, 2014). Since the methanol has bypassed the anode, the transfer of electrons in the reduction-oxidation reaction does not create a potential differential over the cell; only waste heat is the end result. Park et al. (2012) have proposed that crossover can be minimized by inserting a hydrophilic layer between the oxygen feed and the cathode catalyst layer, as well as a hydrophobic layer between the methanol feed and anode catalyst. This would allow the hydrophobic layer to reject water in the methanol feed from migrating through the cell, while the hydrophilic layer would absorb any water which was able to cross over. The combined effect would be to limit the species responsible for crossover and reduction of potential for the cell (Park, et al., 2012).

Rationale for Use of High Temperature

Kinetics of Fuel Cell Reactions

It is known in the field of chemical kinetics that temperature has a significant effect on the rate at which a reaction proceeds (Fogler, 2005). The Arrhenius equation states that the kinetic rate constant (and therefore the rate) will be significantly faster at higher temperatures. For this reason, this report investigates the effect on cell potential and current of a fuel cell

operated at different high temperatures within (and outside of) the manufacturer recommended operating temperature range for the electrolyte used.

$$k(T) = \mathrm{A}e^{-\mathrm{E/RT}} \quad (13)$$

In the Arrhenius equation, *k(T)* represents the reaction rate constant based on the temperature at which a reaction is proceeding. *A* is a pre-exponential factor, *E* is the activation energy for the reaction, *R* is the ideal gas constant, and *T* is the absolute temperature, the independent variable of this equation.

The kinetics of an electrochemical reaction are further predicted in the Butler-Volmer equation which relates the over potential and transfer coefficient to the rate constant (Datta, 2014).

$$k(T) = \mathrm{A}e^{-\mathrm{E/RT}}e^{\alpha \mathrm{F}\eta/\mathrm{RT}} \quad (14)$$

This equation models the kinetic rate constant based not only upon the activation energy and temperature as in the Arrhenius equation but also based on the electrode over potential η. Here F represents Faraday's constant. The Butler-Volmer equation shows that the kinetics of a cell can be increased by increasing the temperature, but also by increasing the overpotential of the electrode. Increasing the temperature should increase the performance of the cell by reducing the overpotential. Another conclusion of this model is that the kinetics of the cell can be increased even at room temperature if one is willing to sacrifice over potential, increasing the value of the second exponential term of the equation.

It has been shown that the kinetics occurring at the anode electrode of a DMFC is slower than those at the cathode anode. For this reason, it is common for the catalyst loading on the anode side to be higher than the catalyst loading on the cathode side (Cho, et al., 2008). The

MEAs used in these tests also follow this pattern, with 0.7 mg of platinum catalyst on the cathode side, and 1 mg of platinum on the anode side (Henschel, 2014).

Use of Polybenzimidazole (PBI)

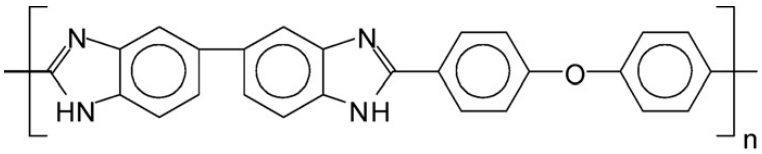

FIGURE 11: POLYBENZIMIDAZOLE MONOMER STRUCTURE (MODESTOV, ET. AL., 2009).

The polybenzimidazole (PBI) polymer imbibed with phosphoric acid (PA) is one option when choosing a membrane material for a high temperature direct alcohol fuel cell because of its high oxidative, hydrolytic and thermal stability (Gubler, et al., 2007) at elevated temperatures. This has been shown by trials in which durability was maintained over a 20,000 hour lifetime. Over this time, a cell was operated at 160˚C with dry H_2/air feed. PBI-PA has been compared to Nafion® -117 for a DMFC, and it was shown that PBI is capable of sustaining performance at higher concentrations of methanol, and with half the observed alcohol crossover. (Gubler, et al., 2007) Thus, this report focuses on the use of Celtec-P1000, the commercially available MEA based on PBI-PA, manufactured by BASF in Germany. The polymer is used to facilitate transport protons from the catalyst across the cell to the opposite electrode. Because free protons are not stable, acid, base or salt ions must be doped into the polymer structure to act as proton donor/acceptor sites (Datta, 2014). It has been found that phosphoric acid is a better candidate than other acidic compounds at higher temperatures because of low volatility (Schuster, et al., 2005), so PBI is often with phosphoric acid in the

commercially available PBI membrane electrode assembly Celtec-P1000 (Gubler, et al., 2007). When doped with phosphoric acid, PBI can transport protons via the Grotthuss (Modestov, et al., 2009)and Vehicle Mechanisms (Datta, 2014) in similar fashion to the transport in Nafion®.

To enable the motion of charges through the membrane layer, polybenzimidazole is doped with phosphoric acid so that hydronium ions can easily form, facilitating both the Grotthuss and Vehicle mechanisms (Gubler, et al., 2007) (Henschel, 2012). The structure of PBI with the bonded acid molecules is displayed in Figure 12. Only two phosphoric acid molecules can be bonded to each polybenzimidazole monomer, leaving most of acid in the membrane electrode assembly to be free acid, which is susceptible to leaching (Gubler, et al., 2007). When the acid is not bonded directly to a monomer site, it can be washed out of the polymer layer in the presence of liquid; therefore, great care must be taken to prevent the presence of liquid water or methanol in the MEA.

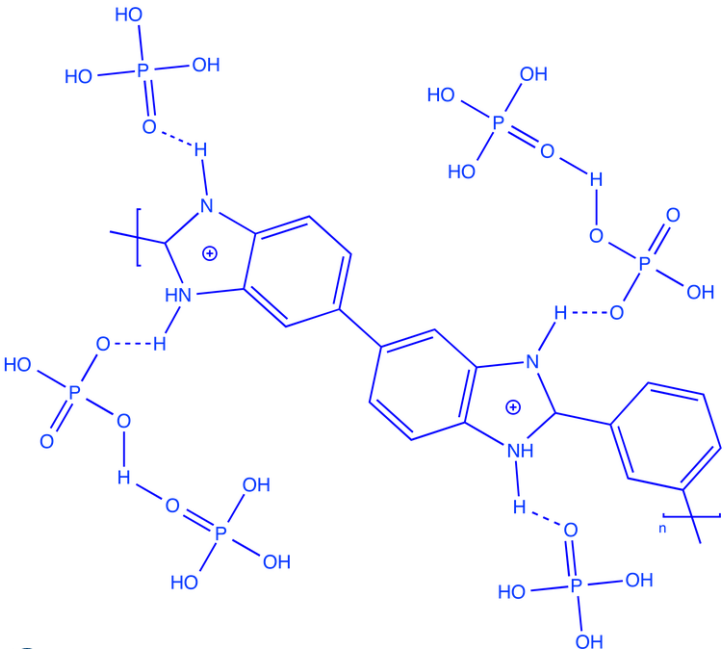

FIGURE 12: STRUCTURE OF PBI SHOWING BONDED ACID MOLECULES ON THE BACKBONE (HTTP://NICHECREATOR.COM/POLYBENZIMIDAZOLES)

The CeltecP-1000 MEA provided by BASF for testing also has the interesting property of a lower-than-standard catalyst loading for a DMFC. While the norm for a DMFC is about 4 mg/cm^2 for the catalyst, this MEA has a loading of 0.7 mg of catalyst nanoparticles on the cathode side, and 1 mg of platinum on the anode, a quarter of what is typically used (Henschel, 2014) since it is designed for reformed H_2 (Figure 1). This makes it possible to reduce the cost of purchasing the materials of construction for a DMFC, assuming that performance comparable to that in a conventional Nafion® DMFC can be achieved.

PBI-PA was selected as the candidate for this research into high temperature methanol fuel cells for its ability to withstand temperatures high enough to improve kinetics. PBI is ideally suited for high temperature operation, as evidenced by research by Gubler (2007) showing the longevity of operation at 160˚C, and the recommendation from the manufacturer that the PBI-based membrane electrode assembly CeltecP-1000 be operated at these elevated temperatures (Henschel, 2014). equation 14, the Butler-Volmer equation shows that the kinetics of an electrode reaction increase with temperature when other parameters are held constant, however because of the free acid present in the PBI polymer layer, the increased kinetics would diminish quickly as any liquid fuel stripped the acid from the layer, greatly reducing the ability of the MEA to facilitate Grotthuss and Vehicle mechanistic motion of protons. It is in this consideration that the ability to run PBI-based MEAs at high temperature shows its true worth. To avoid leaching the acid with a liquid stream of fuel as in conventional DMFC, the high temperature allows the cell to be fed a vaporized flow of methanol which

interacts with the gas diffusion layer in the same way as H_2 gas. Based on literature review, this method of introducing feed material to the cell is not a common one, and therefore deserves due attention, to fully elucidate the potential of polybenzimidazole as a MEA proton-transport material. In the following chapters, we present the method by which tests were carried out on the existing fuel cell in Worcester Polytechnic Institute's Fuel Cell Laboratory, and we show the results of a number of tests which help characterize the performance of the CeltecP-1000 MEA as a DMFC under high temperature and vapor-fed conditions.

3. Methodology

Apparatus

At the heart of the apparatus used for testing is the PBI-based MEAs whose conditions and configurations are manipulated and analyzed. However, there is a large amount of additional hardware that must be used to test under the desired conditions. These range from the temperature controls to the housing of the MEA in the cell and the pump that is used for maintaining a constant even flow for a multitude of methanol concentrations. The full assembly is shown in Figure 13: Testing Station.

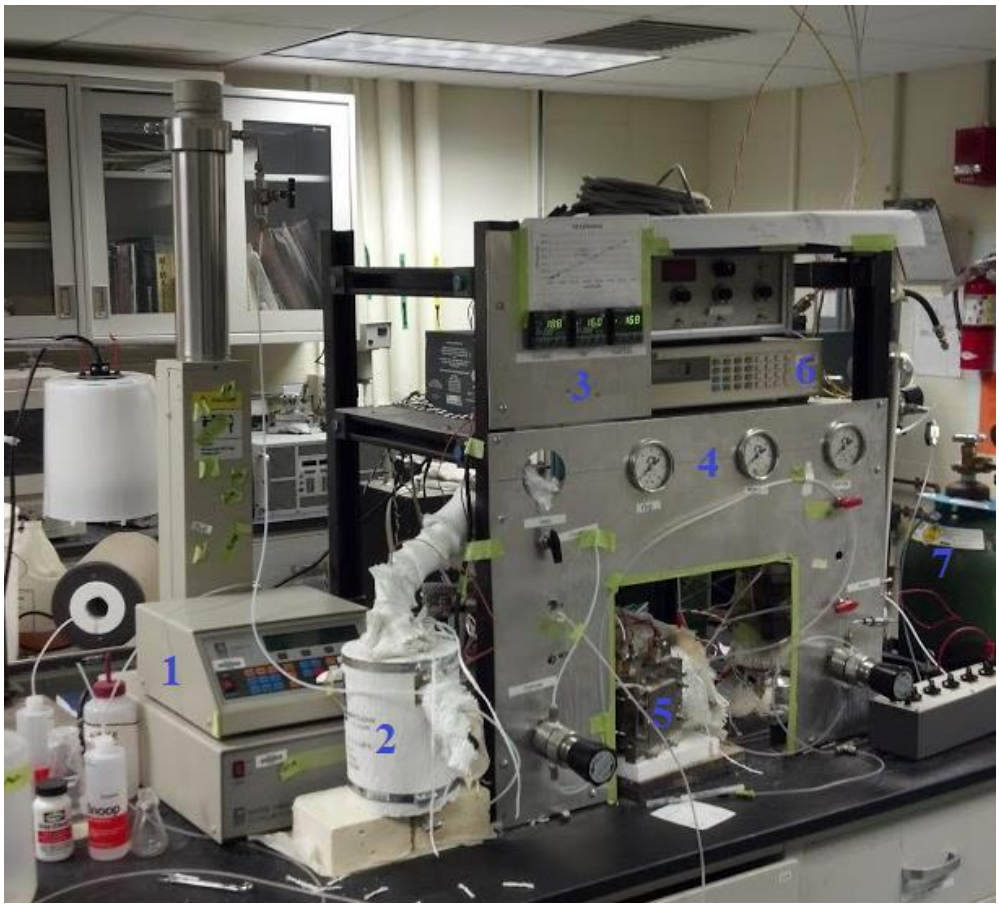

FIGURE 13: TESTING STATION

Initially, methanol-water fuel mixture is stored in the syringe pump (1), which is used to pump the fuel to the cell through the furnace for evaporation (2) via tubes lined with heating tape. The temperatures of the furnace, the feed line from the furnace to the cell and the cell itself are controlled via digital temperature controllers (3) mounted on the apparatus housing. The pressures of the methanol feed, oxygen feed and (if need be) the hydrogen feed are measured with the analog gages seen as item (4) in Figure 13. The cell itself is at the center of the system (5) fed by the methanol and oxygen feeds and heated by heating tape. When the electrode reactions proceed in the cell, the electrons liberated at the anode are channeled through a load box (6) which allows us to monitor the electrical output and adjust the amperage and voltage as needed to conduct tests. The final item in Figure 13 is the oxygen tank (7) from which gas is fed to the cell to facilitate the cathode reaction.

At the center of the fuel cell is the MEA which was commercially fabricated by BASF. To begin, the anode side of the cell assembly was placed with the internal side facing up exposing the channels in the graphite block (Figure 14). Ceramic dowels were placed into two holes at opposing ends of the anode blocks to ensure that the pieces of the cell would be aligned properly and maintain a constant position. Two gaskets, provided by BASF with openings matching the area of the gas diffusion layer (GDL), along with the MEA itself were then punctured with a circular die to match the position and size of the rods in the anode. This ensured that the flow of the channels would not be impeded by any overlay. One of the gaskets was then placed over the rods and set into position against the graphite block of the anode side. Following the first gasket, the MEA was carefully lowered into position followed by the second gasket ensuring that the GDL was fully exposed to the channels. The cathode was then

lowered into position guided by the dowels onto the top gasket. Eight bolts were placed through the edges of the cathode (two on each side) and anode and tightened in a star pattern to ensure an even seal. The gaskets were used to prevent over compression and ensure a leak-proof seal when testing.

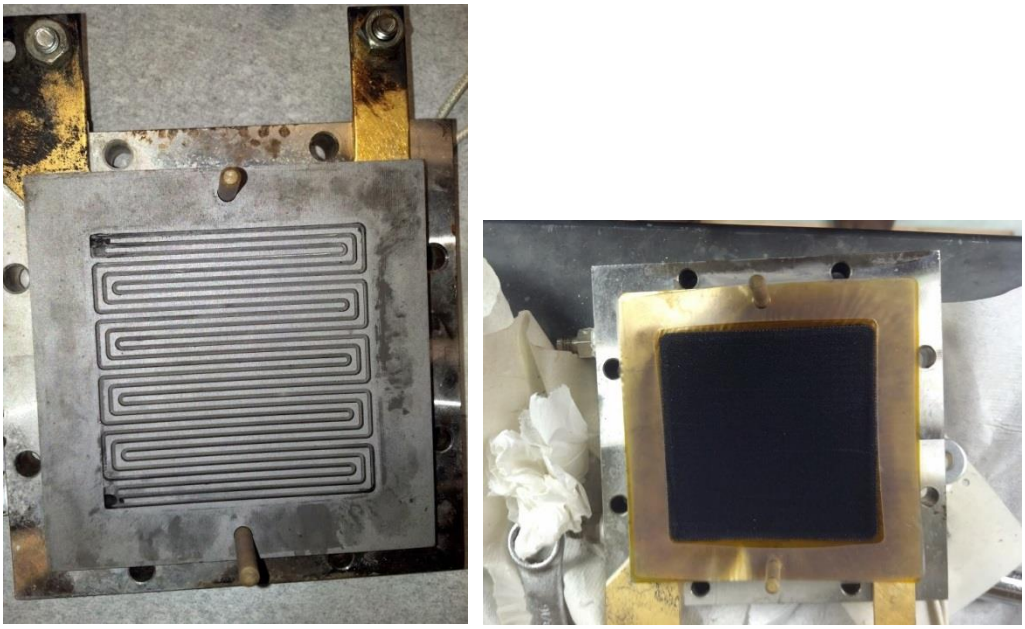

FIGURE 14: FUEL CELL DISASSEMBLED

Once assembled, the cell was placed on a thermally neutral block under the test station and connected to a load box with small bolts as shown in Figure 15. A thermocouple was placed into the cathode side to provide temperature data to the control box operating heating plates that were on both the anode and cathode side of the cell as can be seen on the bottom left of Figure 15.

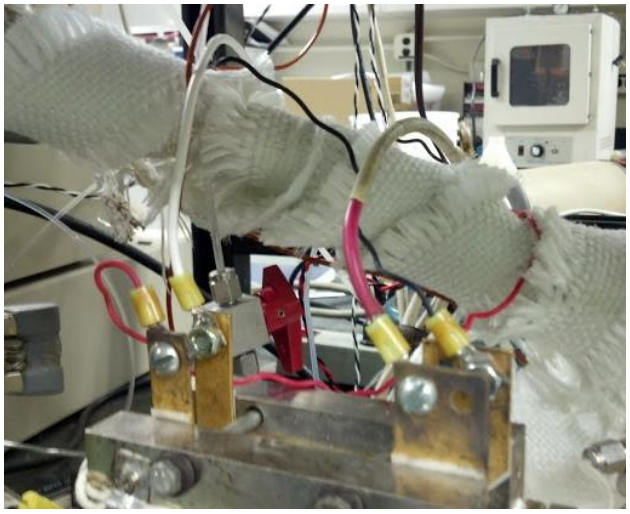

FIGURE 15: CELL ELECTRICAL CONNECTIONS

Feed lines were connected to the top two inlets of the apparatus and waste lines to the bottom of both the anode and cathode sides as shown in Figure 16: Cell Line Connections. The plates were plugged into an electric plug that was controlled by a thermal controller next to the load box to maintain cell temperatures.

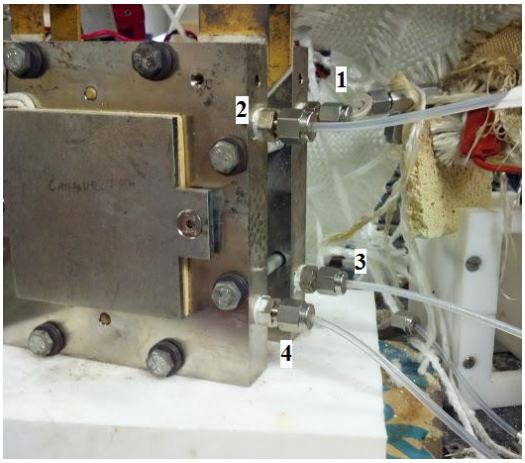

1 – Methanol Inlet

2- Oxygen Inlet

3- Anode Outlet

4- Cathode Outlet

FIGURE 16: CELL LINE CONNECTIONS

The flow of methanol was controlled by a pump which allowed the flowrate to be set to 1.5 mL/min for testing (Figure 17). To fill the pump reservoir the tubing connected to the pump would be placed into the alcohol solution being tested and refilled at between 150 to 200

mL/min. After the pump had stopped refilling, the line remained in the solution for an additional few minutes as the suction had lowered the pumps internal pressure from 16-18 psi to around 6-9 psi and thus would continue in taking liquid until the pressure was restored. A flow of 100 mL/min was then run through the pump until liquid flowed from the mouth of the tubing back into the bottle being used to store the liquid ensuring that the line was fully charged with alcohol and did not contain any air. Once the pump reservoir had thus been filled, it was connected to the furnace and set to run at 1 mL/min for activations. Activation of the cell typically lasted four hours during which time the cell was fed a reduced amount of alcohol before variable loads were applied to the cell in tests. The pump duty was changed to 1.5 mL/min for the actual load tests. After the testing of one concentration was completed, the pump was emptied and filled with distilled water to clean and maintain the system before a new concentration was added.

FIGURE 17: PUMP DIAGRAM

The furnace is run via a controller that can be manipulated to a targeted set point temperature. At lower temperatures, the controller maintains a calm response to change only varying by a couple of degrees. However, at high temperatures above 220 degrees Celsius the controller fluctuates rapidly. At the bottom of the furnace the pump is attached to feed liquid into the system. The top of the furnace flows out the heated vapor into metal tubing leading to the feed line. Before the vapor is fed to the cell itself, its temperature is controlled once more by heating elements in the feed line working off of data collected by thermocouples in the line.

Activation of PBI-Based MEA

The Membrane Electrode Assemblies used in this report were Celtec P-1000 polybenzimidazole-based hydrogen fuel cell assemblies fabricated by BASF in Germany. These MEAs are manufactured to have 50 cm^2 of surface area, and are square, meaning that each side is about 7.1 cm. Surrounding the gas diffusion layer is a plastic liner which serves to hold the MEA in place when pressure is applied upon tightening of the two halves of the cell. The catalyst layer of the MEA contains 0.7 mg of platinum/nickel alloy on the cathode and 1 mg of platinum black on the anode catalytic surface (Henschel, 2014).

Prior to testing, activation of the PBI-Based MEA was performed in accordance with the BASF provided instructions. The MEA was loaded into the fuel cell as above and brought to a temperature of 160˚ C. Hydrogen was connected to the anode and oxygen to the cathode with both having an established flow at 2 psi. BASF's instructions contain a recommendation that activation be conducted at 0.09 amps per cm^2, so a total load of 4.5 amperes was placed on the 50 cm^2 MEA for a total of 50 hours. Over the time, the MEA's amperage increased until a

steady value was achieved at roughly 50 based on BASF's recommendation and provided activation graph shown in Figure 18.

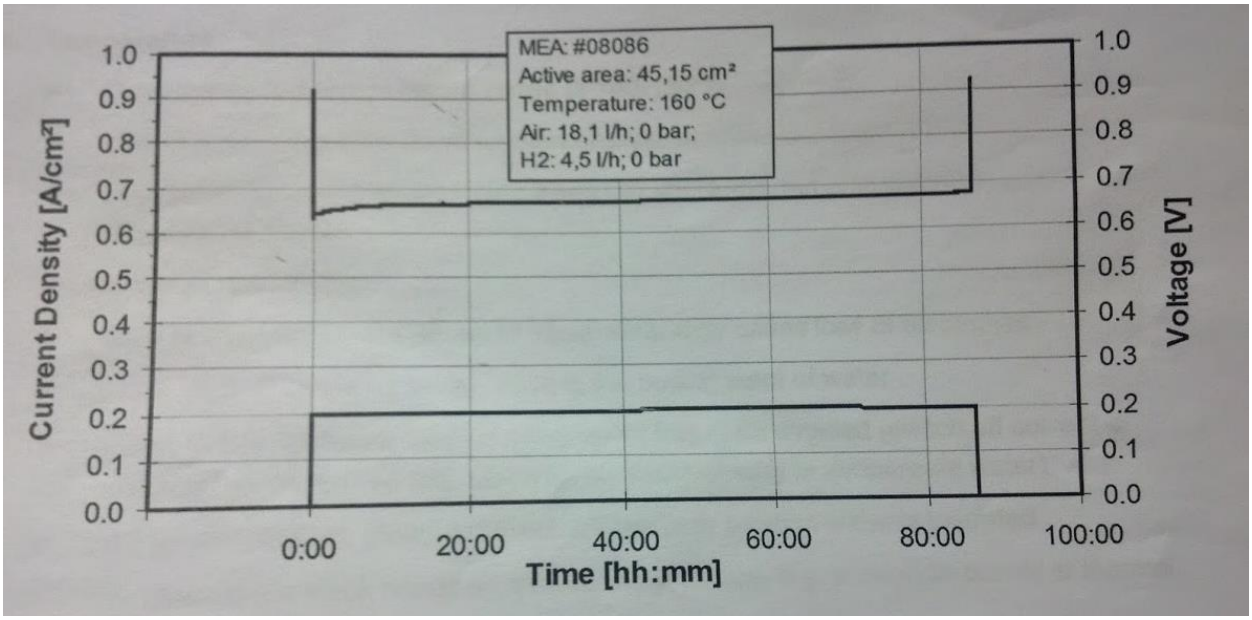

FIGURE 18: BASF HYDROGEN ACTIVATION GRAPH (HENSCHEL, 2012)

The hydrogen feed was then switched to methanol flowing at 1.5 ml/min with oxygen feed varied to match the pressure, typically about 2 psi on both sides. The load on the cell was placed at 1amp for this portion of the activation. This methanol-oxygen activation continued for a minimum of 18 hours before testing occurred. The hydrogen activation ensured that the MEA was fully activated and ready to begin taking a load, and that it had reached steady state in its operational capacity. The methanol activation was meant to distribute methanol across the entire active area of the cell so that it was ready to begin amperage-variation testing with a methanol feed.

After a test was complete, the cell was placed onto nitrogen by attaching a nitrogen tank to both feed lines ensuring equal pressure. This allowed the cell to be stored in an inert environment overnight between tests. To ensure that the cell was fully activated after this

period of sitting in an inert environment, a smaller activation was used when the cell was brought to temperature along with the feed line and the furnace to allow methanol of the desired concentration to be vaporized. Once vaporization was complete, the nitrogen was removed from the cell and methanol added to the anode side with oxygen added to the cathode. The cell was then placed under a load of one volt for four hours before testing began. BASF recommended that the cell undergo a miniature activation after being in a nitrogen atmosphere to ensure that the cell was at steady state, and not in the process of re-acclimating to a methanol feed. This time frame was determined early in testing through monitoring the power density over time resulting in a consistent power density curve at four hours.

Testing of PBI-Based MEA

Single MEA

The initial data sets taken to establish a baseline performance for the cell were taken with a stock MEA configuration. This configuration consists of applying the MEA as it is packaged by BASF without any modification. When delivered by BASF, the MEAs consist of a single gas diffusion layer on the anode and cathode sides. The total thickness of the assembly is typically around 850 microns, though some variability is observed (plus or minus no more than 5%). To test the performance with this setup, the apparatus was run at several temperatures, and several concentrations of methanol in water. The temperature tests were performed to establish the role of kinetics in the electrical output that the cell was capable of. Initially the cell was run at temperatures of 160, 170 and 180˚C, as these represent the higher end of the temperature range recommended by BASF (company literature recommends operating between 140 and 180˚C). Once the trend for these temperatures was established, it was

decided to push the cell beyond the advisable temperature range to find the point at which increased kinetics are overcome by damage to the MEA by the excessively high temperature. To this end, the MEA was subjected to tests at 200, 220, and 240˚C, though the highest of these temperatures was abandoned quickly when it was found that this temperature causes damage to the MEA, rendering it inoperable. The concentration of methanol in water was altered for the tests to see if a higher concentration could be tolerated at elevated temperatures. Due to time constraints, the flowrate of solution was held constant at 1.5 mL/min, i.e. the effects of flowrate were not investigated here.

When each set of operating conditions was decided, the cell was brought to these conditions and testing commenced. The cell and methanol feed line would be adjusted using controllers to the temperature of interest for a test, and the furnace which heats the methanol would be brought to some temperature slightly above that of the cell to account for cooling in the 1/8'' teflon transport lines. The cell would be brought from its inert condition of nitrogen atmosphere to a state of being fed methanol and dry oxygen. The flow of nitrogen would be stopped using the control valve on the nitrogen tank, and the nitrogen lines would be disconnected from the inlets to the cell, and replaced by the heated methanol feed line on the anode, and by the oxygen line on the cathode. The syringe pump containing the reservoir of methanol solution would be turned on to a flowrate of 1.5 mL/min. When methanol was observed to flow into the cell, the oxygen feed would be turned on by the control valve located on the compressed oxygen tank. Only when both methanol and oxygen were flowing to the cell would be load box be turned on, because the box will pull a load on the cell even if there is no

fuel, meaning that current would have to be developed from the motion of electrons derived from the MEA layer components, causing rapid degradation.

When this configuration is achieved, the cell would be monitored to ensure that it has reached stable conditions, and then left for four hours before testing began to ensure that the catalyst and PBI layers were at steady state and fully populated with methanol. To establish the polarization curves which define the cell's performance, readings would be taken of the current resulting when various voltages are imposed on the apparatus. These readings would be recorded and plotted as current density versus voltage and current density versus power density. The current density is calculated by taking into account the current output of the cell, and the known active area of the MEA gas diffusion layer, 50 cm^2. The power density is calculated as simply the current density multiplied by the voltage across the cell. With plots of this data, it is possible to establish the performance trends presented and discussed in Chapter four.

Internal Reforming using internal reforming layer

Internal reformation or pre-reformation of a fuel feed to a cell is one method currently under investigation for improving the performance of fuel cells. When a fuel is reformed it is made to partially react before reaching the catalyst layer of a fuel cell. This can be done outside of the cell, in the case where another piece of equipment is used to react the fuel before it is fed to the cell (Figure 1), or inside the cell, where an extra layer of catalyst could be added to react the fuel between the feed and the MEA. Thus, Agouropoulos (2012) conducted experiments in which a methanol was pre-reformed with a copper-based catalyst placed

adjacent to the membrane electrode assembly (Avgouroloulos, et al., 2012) . In these experiments, it was shown that the addition of the extra catalyst “significantly improves the electrocatalytic behavior” observed in the cell. Based on this initial evidence, it was decided to preliminarily test a system of internal reforming in the laboratory-scale fuel cell used in preparing this report. To test the effects of pre-reforming the methanol fuel, an extra catalyst layer was added to the anode electrode between the feed and the normal catalyst. The added catalyst layer was simply and anode GDL with catalyst layer taken from a previously used MEA manufactured to the same specifications as the normal MEA. The spent MEA was removed from the cell after experiments had been performed on it, and the anode gas diffusion layer and catalyst were peeled off from the old MEA and added to the anode of the new with the catalyzes layer directly exposed to the incoming methanol feed. The orientation of the GDL allowed the fuel to contact a catalyst layer immediately upon entering the cell environment. To prevent the channels of the plate from damaging the catalyst, an extra gasket was added to the anode to provide extra cushioning between the plates as they were tightened.

Throughout testing, and literature research, it was quickly established that increasing the temperatures at which the cell operates can have a profound effect on the power output of the cell. Literature provided by the MEA manufacturer, BASF states that the operable range of temperatures for the PBI-based Celtec-P1000 is 140-180˚C (Henschel, 2012). To establish trends within this range, tests were initially run at 160, 170 and 180˚C in sequence with the same batch of concentrated alcohol. These tests were run while the stock MEA was in use, as well as once the internal pre-reforming was instituted. After improved performance was seen, the methodology was modified to include comparative tests performed at higher temperatures

than those recommended by the manufacturer. It was assumed that longevity would be issue in this range but, that short-term performance would continue to increase as the temperature was increased to a certain damage point. To try to establish this point, the cell was run under identical concentration conditions but at temperate of 200, 220, and 240˚C in sequence. As the high temperature tests were carried out, it was observed in one test that an acrid vapor (possibly smoke) emanated from the cell at the conclusion of testing. After this, the cell no longer performed at the level expected. At this point it was necessary to exclude temperature tests at and above 220˚C.

To provide understandable trend analyses, the data collected were organized into sets of varying methanol concentration at constant temperature, and alternatively, the data collected in tests at different temperatures run on a single concentration. At certain points, the validity of data were brought into question because of possible degradation of a given MEA, so runs were also carried out for the sole purpose of confirming data previously collected. In these cases, if the newly collected data was deemed more valid than a previous set because of potential degradation of an MEA, it would be taken as a replacement with the old set abandoned. Only the results of those valid tests are included in this report.

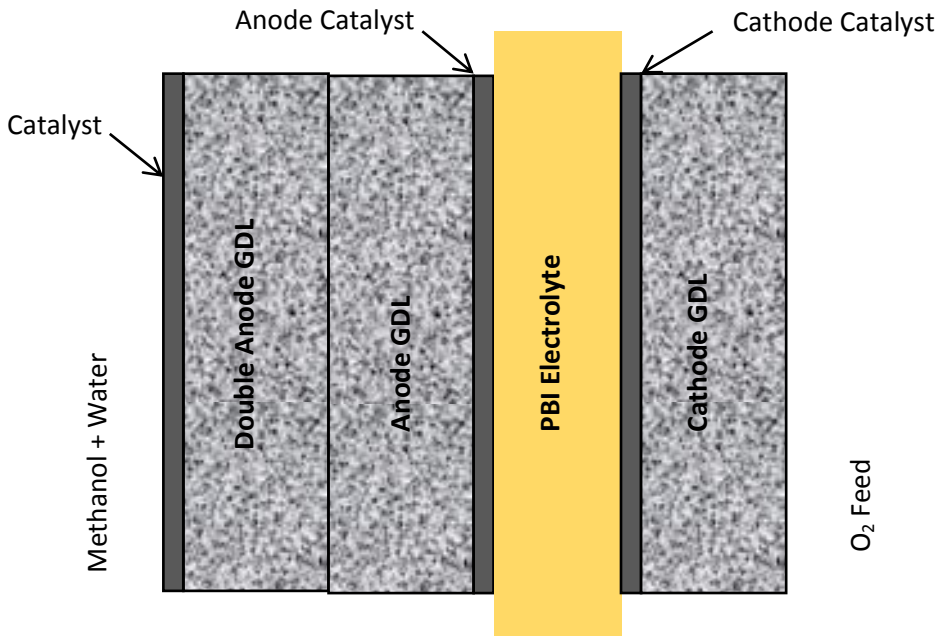

FIGURE 19: SCHEMATIC OF FUEL CELL WITH A DOUBLE ANODE (DA) LAYER FOR INTERNAL REFORMING

4. Results and Discussion

A multitude of conditions were tested to determine trends that would lead to the optimal performance parameters for the high temperature direct methanol fuel cell. The major conditions tested were that of fuel concentration, temperature, and the inclusion of an internally reforming layer on the anode side of the MEA. Solutions of 3, 5, 7.5, 10, 17, and 27 (neat) molar methanol in water were prepared for testing to establish trends for the full range of fuel concentrations which could be fed to the apparatus. Initially, 1M solutions were also prepared and run through the cell, but greatly reduced performance was observed, leading to the conclusion that this concentration contained so much water that there was not enough methanol fed to the fuel cell. The recommended range of temperatures for the PBI membrane electrode assembly is 140-180˚C, thus testing began within this range with data collected at 160, 170 and 180˚C. Once it was observed that performance of the cell increased with

temperature increase in this range, it was decided to push the system beyond the recommended limits to establish at what point temperature-dependent increases would stop. To this end, the apparatus was tested at 200, 220 and 240˚C until damage was observed. The final set of tests included the addition of a second catalyst/gas diffusion layer component to the anode side of the apparatus to pre-reform the feed of methanol. In these tests the performance of a standard BASF membrane electrode assembly was compared to the performance of the same setup with the extra layer manually added. Due to time constraints, the flow of methanol was kept consistent at 1.5 mL/min and oxygen was varied to match the pressure produced by the methanol flow. No experiments were conducted with our feed to the cathode. The results below are not necessarily in the order in which they were conducted.

Temperature Effects

The experiments to determine the temperature dependence of performance at each concentration was run at the temperatures recommended by the manufacturer, as well as above the highest recommended temperature. Figure 20 displays the trend of performance for 3M methanol at temperature ranges 180-240C.

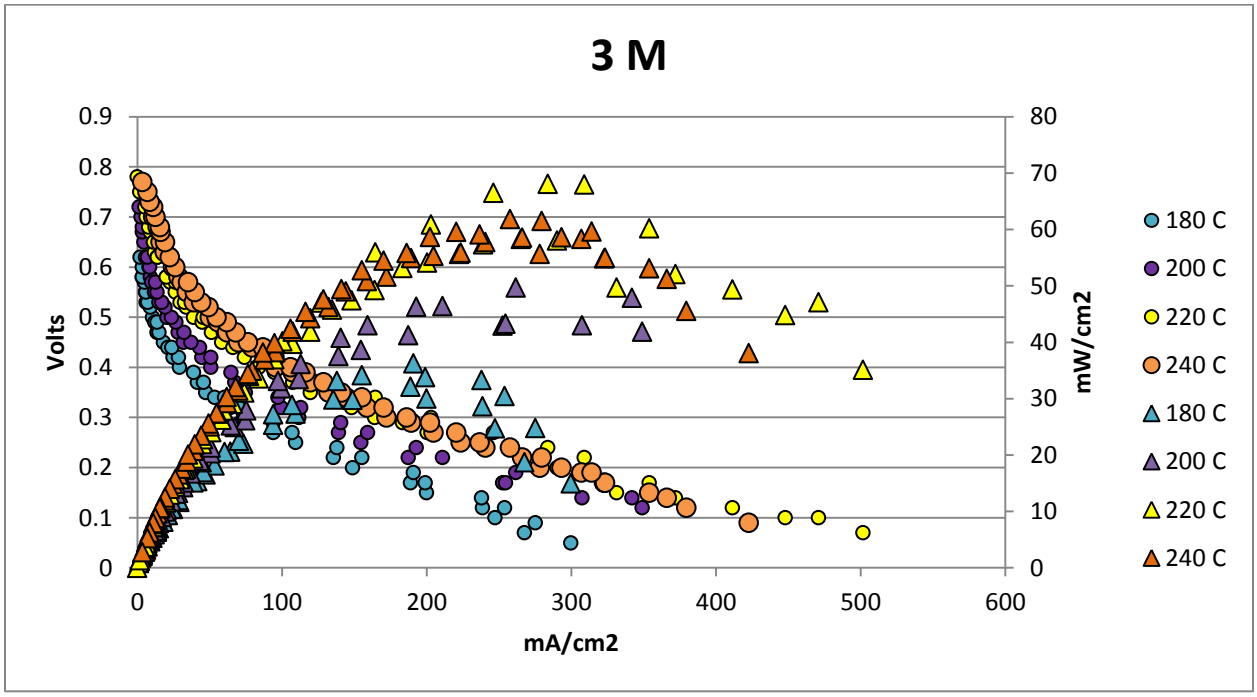

FIGURE 20: POLARIZATION PLOT OF 3M METHANOL AT VARIOUS OPERATING TEMPERATURES

It was expected based on kinetics that the higher temperatures would produce a greater current and power density as shown by the elongated curves at higher temperatures. During data collection, it was noted that there was a heavy oscillation in readings at lower voltages of which the rough average was taken. It is theorized that these are due to catalyst poisoning and cleansing cycles as discussed above. At higher temperatures these oscillations increased in size and caused a fluctuation in both amperage and voltage at lower current. The recommended temperature for the cell was 140-180˚C which was tested before the new test of above

recommended temperatures. While operating at 200˚C the power density curves are tightly grouped. At 220˚C the trend became scattered but returned at 240˚C to a fairly consistent power density curve. Upon removal of the methanol feed line from the anode side of the cell, a small but noticeable puff of smoke exited the fuel cell during the process of placing the cell into an inert state using nitrogen for storage between tests. After the smoke was observed, tests were conducted to determine if damage to the MEA had occurred. Test were thus conducted with a 10M concentration shown in Figure 21.

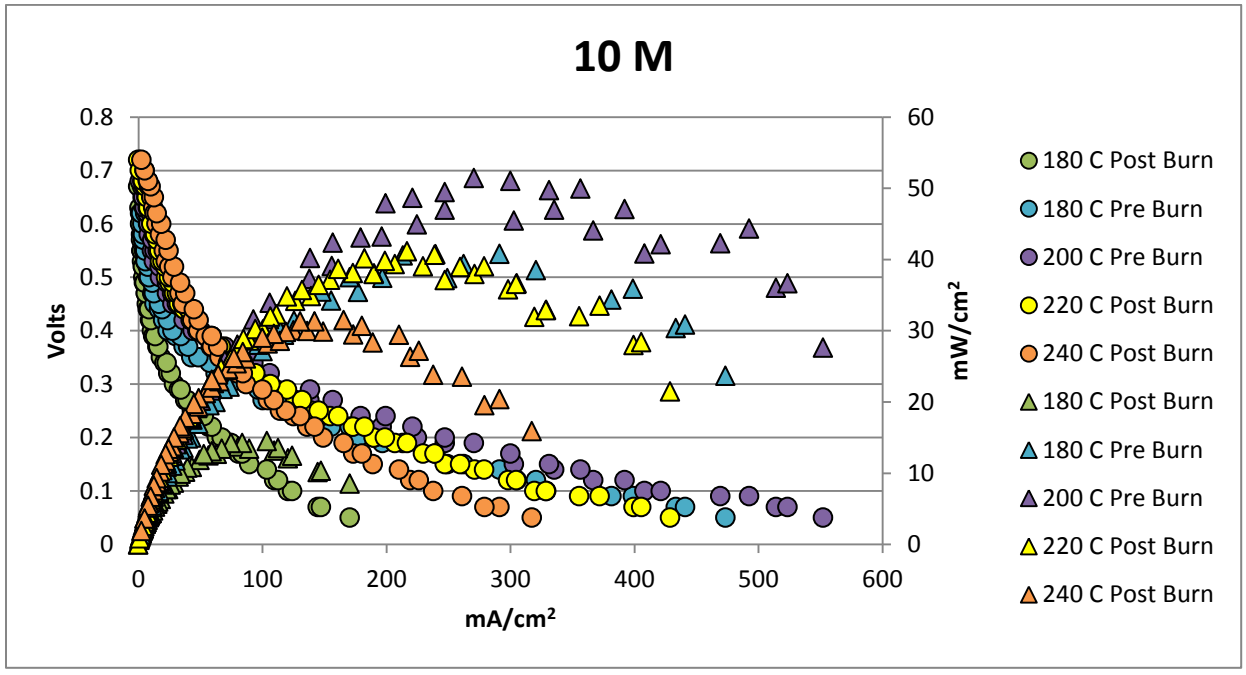

FIGURE 21: COMPARISON OF PERFORMANCE BEFORE AND AFTER SMOKE WAS OBSERVED IN THE CELL. TESTS RUN AFTER THE BURN EVENT ARE OUTLINED IN RED.

When comparing the trends of temperature found in 3M with that of 10M, a significant decrease in both current and power density was observed. It was not clear if this decrease was the result of the damage which may have occurred or another factor, however. It was argued that while values for 220 ˚C and 240 ˚C may be near one another, the resulting values should be

above the value previously recorded (pre-burn) for 200 ˚C. This however was not the case, with both 220 ˚C and then 240 showing results significantly below those for 200˚C. To confirm that this was due to an issue with the MEA itself, the temperature was lowered to 180 ˚C, within the normal operational temperature, and the cell was tested once again to compare to similar tests performed at this temperature before the burn event. It was found to be extremely diminished with a power density peak of around 14 mW/cm^2 just before 100 mA/cm^2 compared to the pre-burn value of around 220 mA/cm^2. In an attempt to determine what was causing the reduced performance with the MEA, the cell was taken apart. When previous issues with performance were observed, dismantling the cell had revealed a chalky, off-white substance that blocked the inlet of the cell as shown in Figure 22.

FIGURE 22: RESIDUE FOUND TO BE BLOCKING THE GAS INLET TO THE CELL (UPPER RIGHT OF SERPENTINE CHANNEL CONFIGURATION)

This issue presented itself by a continuous increase in pressure on the anode side inlet causing testing to be halted for the channels to be cleaned and a new MEA to be activated. The MEA also displayed this caking when the blockage issue occurred as shown in Figure 23.

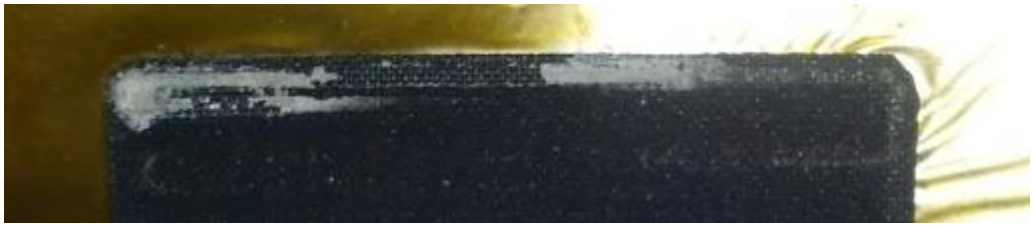

FIGURE 23: BLOCKAGE OBSERVED ON THE GAS DIFFUSION LAYER OF THE MEMBRANE ELECTRODE ASSEMBLY.

It was theorized that these buildups were due to a liquid feed periodically entering the cell at the inlet due to ineffective evaporation, which caused leaching of the phosphoric acid from the PBI layer, blocking the channels. However, in the case of the issue experienced by the high temperature 3M test, the issue was confirmed by low current densities in the 10M follow up test above 200˚C, and there was no pressure increase on the anode side. It was suspected that the phosphoric acid may have vaporized at these very high temperatures, or that the temperature may have damaged the structure of the PBI making it less able to propagate protons to the cathode. Upon opening the cell, it was discovered that while there was some caking on the MEA as shown in Figure 24, the channels were clear enough to not impede flow and nothing was melted within the GDL layer. It is possible that the significant decline in performance after operating at 240 ˚C is due to vaporization of phosphoric acid from the MEA.

FIGURE 24: CAKING OF MEA POST BURN

FIGURE 25: BLOCKED SERPANTINE CHANNELS IN THE GRAPHITE PLATE

An interesting pattern for what had caked onto the MEA through the testing appeared on the anode side of the cell. While each previous pressure blockage had produced caking, it was limited to the first channel with some minimal amounts in later channels. In the post high temperature MEA however the white material is shown to be all the way to three layers down (more evident than in picture). One possibly mechanism for this result is that vaporization of phosphoric acid followed by subsequent cooling deposited the chalky material more uniformly in channels.

This explanation is supported by the following observation. Along the edges of the cell, the orange PBI material which encircles the GDL layers showed ribbing possibly due to the high

temperature of 240˚C. There were what appeared to be burn marks around the GDL as well. These possible damages due to high temperature coupled with the smoke that was observed and the operating temperature being 60˚C above the 180˚C limit combine to imply that the 240˚C temperature lead to the catastrophic failure of the cell. Consequently, the cell operating limit is below 240 ˚C.

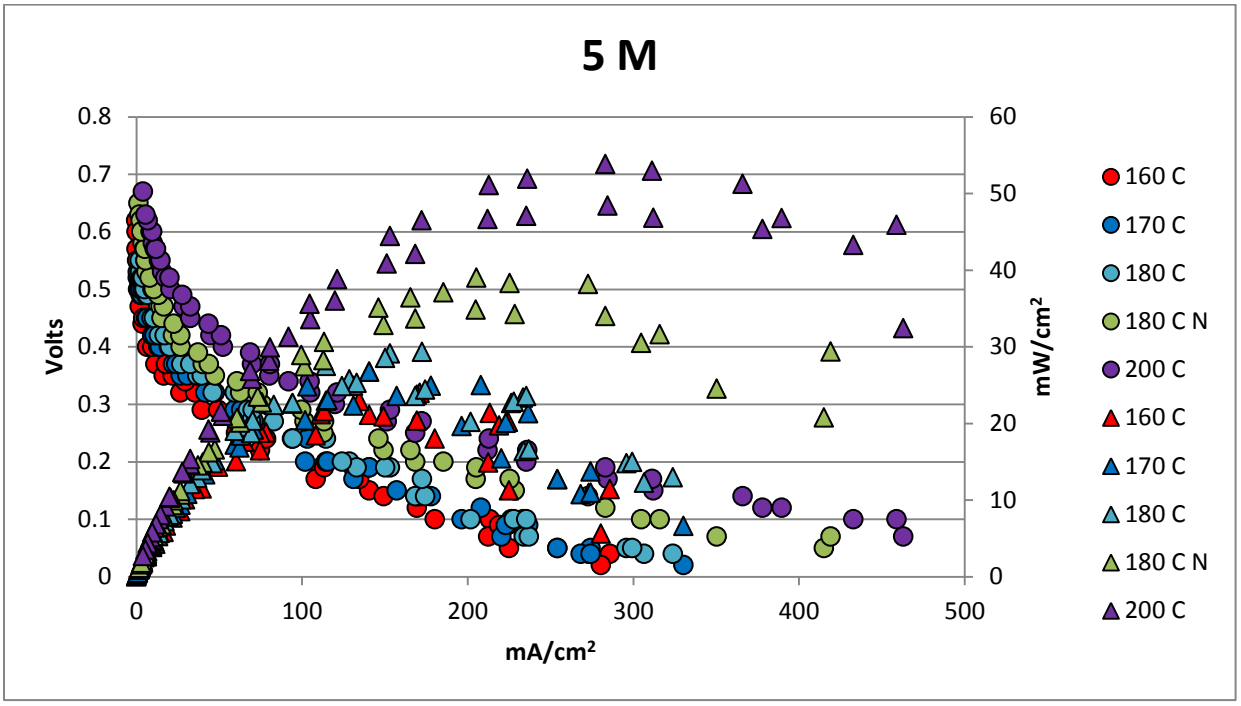

FIGURE 26: PERFORMANCE OF CELL UNDER 5 MOLAR METHANOL FEED, AT VARIOUS TEMPERATURES (N INDICATES A LATER ITERATION OF THE SPECIFIED TEMPERATURE TEST).

As with the 3 M, the 5 M methanol feed showed significant increase with temperature for both the current and power density. As seen in the 3 M experiments, the initial 160, 170 and 180 ˚C results are grouped close together with the most drastic improvement being at 180N and 200 C. The difference in grouping patterns might be attributed to the different MEA's that were used for experiments with temperatures from 160-180 ˚C were collected on MEA's that had been used throughout multiple experiments while the higher temperature values of

180N and 200 were collected with a different batch of MEA's that was ordered separately. To show the difference between the two, the temperature of 180 was tested for each MEA with the new MEA's 180 C reading noted by 180N for 180 new. Though it is true that this result negates the possibility of a direct comparison between temperatures for the two different sets of MEAs, it does allow for the conclusion that temperature does in fact increase the kinetics and performance of the cell when tested beyond the manufacturer-recommended range. This large rise between 180N and 200 can be explained by an increase in the kinetics inside the cell at higher temperatures. While crossover may increase due to the increased electrode kinetics as shown by lower OCV at higher temperatures, the effect that the temperature has on the reaction rate outweighs the effects of crossover, and a net increase in performance is observed.

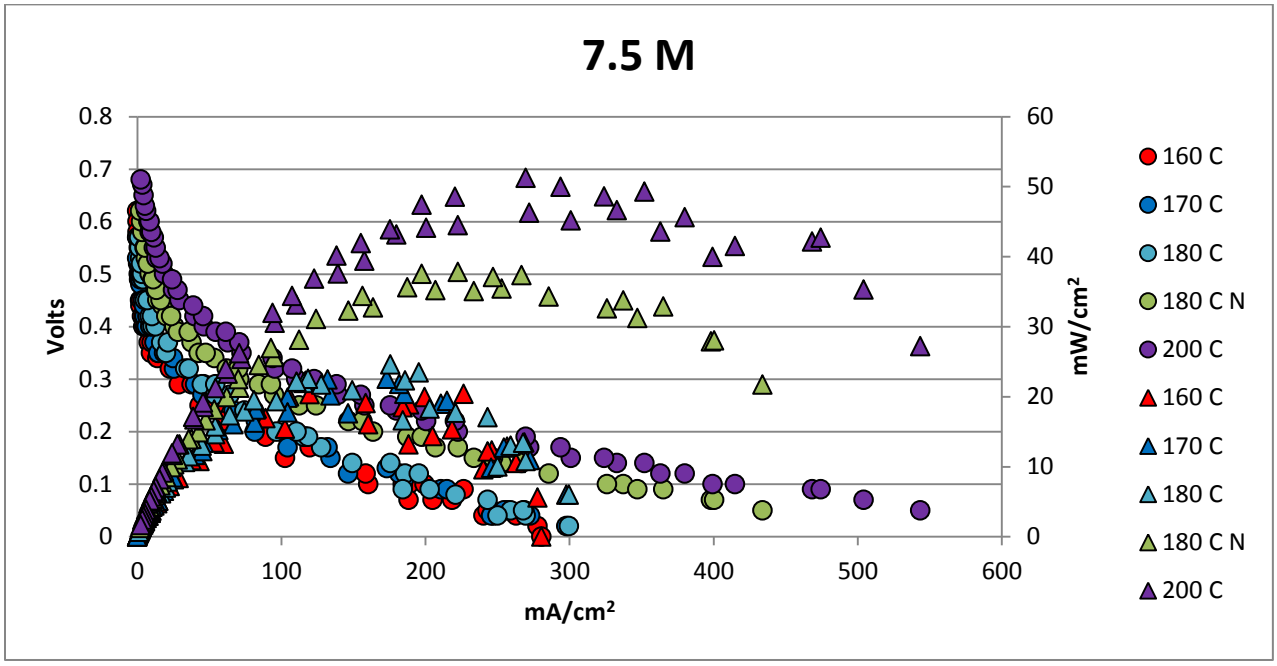

FIGURE 27: PERFORMANCE CURVE OF 7.5 M METHANOL AT A FEED RATE OF 1.5 ML/MIN AT VARIOUS TEMPERATURES

Figure 27 shows the effect of temperature on the performance with a 7.5 M methanol feed. As in the previous results, the power density and current densities are both shown to increase dramatically with the increase in temperature. The same principles hold true for why this occurs as the reasoning behind the 5 M and 3M results. Once again the graph displays data that was collected on two different sets of MEA's with the older MEA set being the tightly clustered 160-180 ˚C, and the new MEA displaying the significant increase between 180 ˚C new (180N) and 200 ˚C.

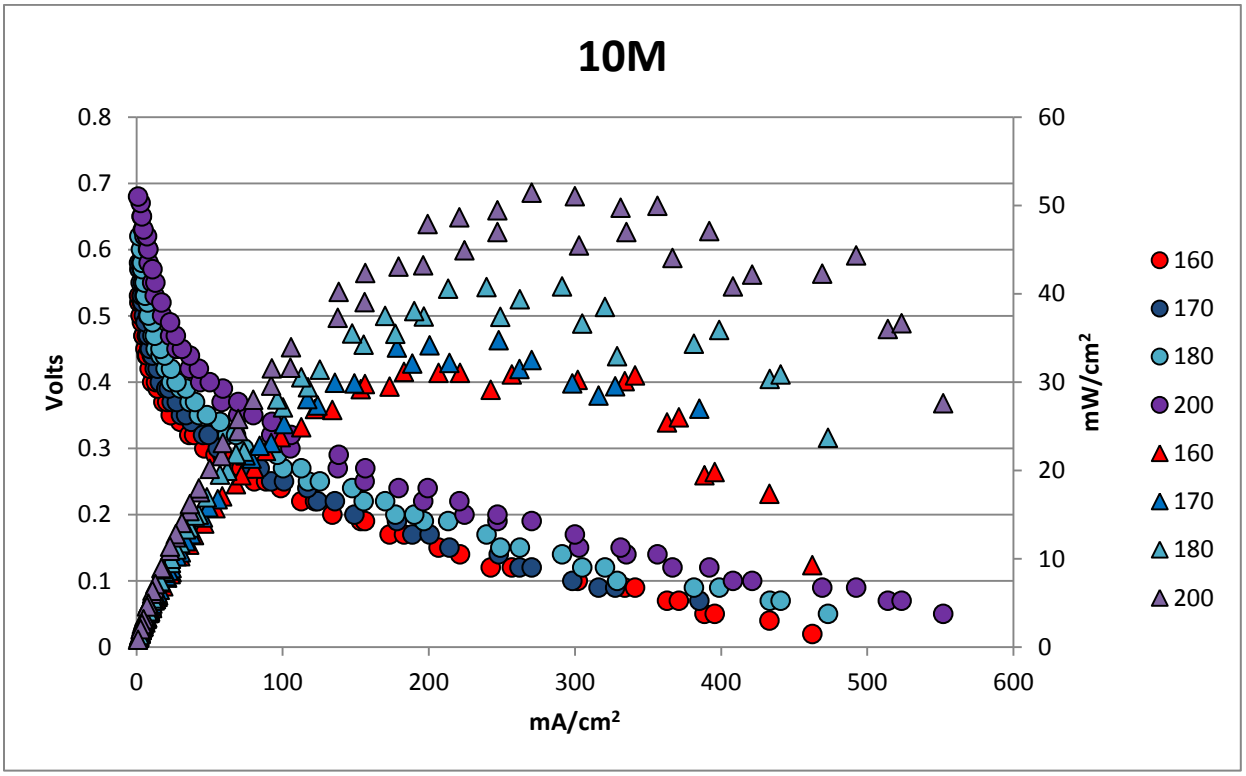

FIGURE 28: THE RESULTS FOR VARIED TEMPERATURE UPON A 10 M CONCENTRATION FEED AT 1.5 ML/MIN

Figure 28 is a true representation of the effects of temperature on a direct methanol fuel cell. All of the experiments were run on the same MEA and confirm the previous results with lower molarities showing that an increased temperature leads to an increased power and current density. At the lower temperatures of 160 and 170 there is only a slight difference with

a barely noticeable difference in mW/cm^2 and almost no difference in the peak mW/cm^2. The 170 ˚C test was stopped short of the others in the test because of instability in the readings. During the experiment, the load box readings would vary as a result of catalyst fouling and clearing cycles, especially at the extremes leading to a limit not set by the cell but rather the limitations of the equipment. At the higher temperatures of 180 and 200 the performance noticeably improved even though the limit of the recommend operating temperature is 180˚C. This is presumably due to lower extent of fouling by CO at the higher temperatures. While the increased kinetics allow for a higher performance output, further testing would have to be done in order to fully understand the effects on the longevity of the cell at the higher temperature, as it is more likely to have faster degradation or face other dire consequences of the higher temperature of operation, such as catastrophic failure.

Molarity Effects

The two largest factors on a direct methanol fuel cell performance are the feed and the operating temperature. In addition to testing varying temperatures, varying concentrations at the same temperature were compared to analyze the performance and to determine the optimal feed conditions for the fuel cell. Due to the knowledge that higher temperatures produce higher power and current densities, high temperatures were the focus of this part of the study, and results of the comparisons of various molarities at lower temperatures are omitted here. Figure 29 shows the performance curves of methanol concentrations 3, 5, 7.5 and 10M at a temperature of 180˚C, the maximum recommended operating temperature.

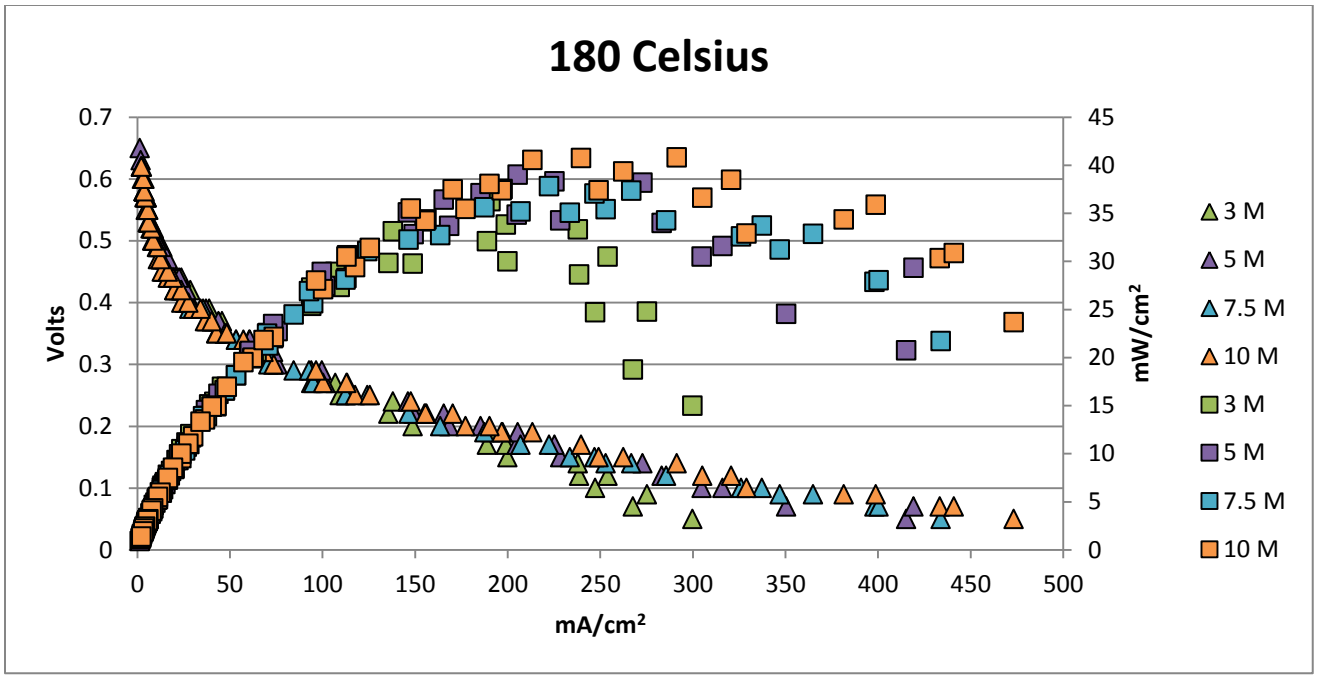

FIGURE 29: RESULTS OF VARIOUS METHANOL CONCENTRATIONS AT 180˚C

The performance of the cell was as expected with very similar current and power densities but an increase at higher concentrations. This increase is because there is more fuel in the higher concentrations for the cell to work with. Indirectly, the 3M concentration for this series allowed for an additional factor to be shown: flow rate of the methanol feed. The pump was mistakenly placed on 1 mL/min instead of 1.5 mL/min producing a drastic reduction in the current density but not in the power density. In other words, it appears that the results are strongly affected by feed flow rate, a variable that was not investigated here. Thus, it is possible that at the flow rate used (1.5 mL/min), the concentration varied markedly between the inlet and the outlet especially at the lower concentrations, affecting performance.

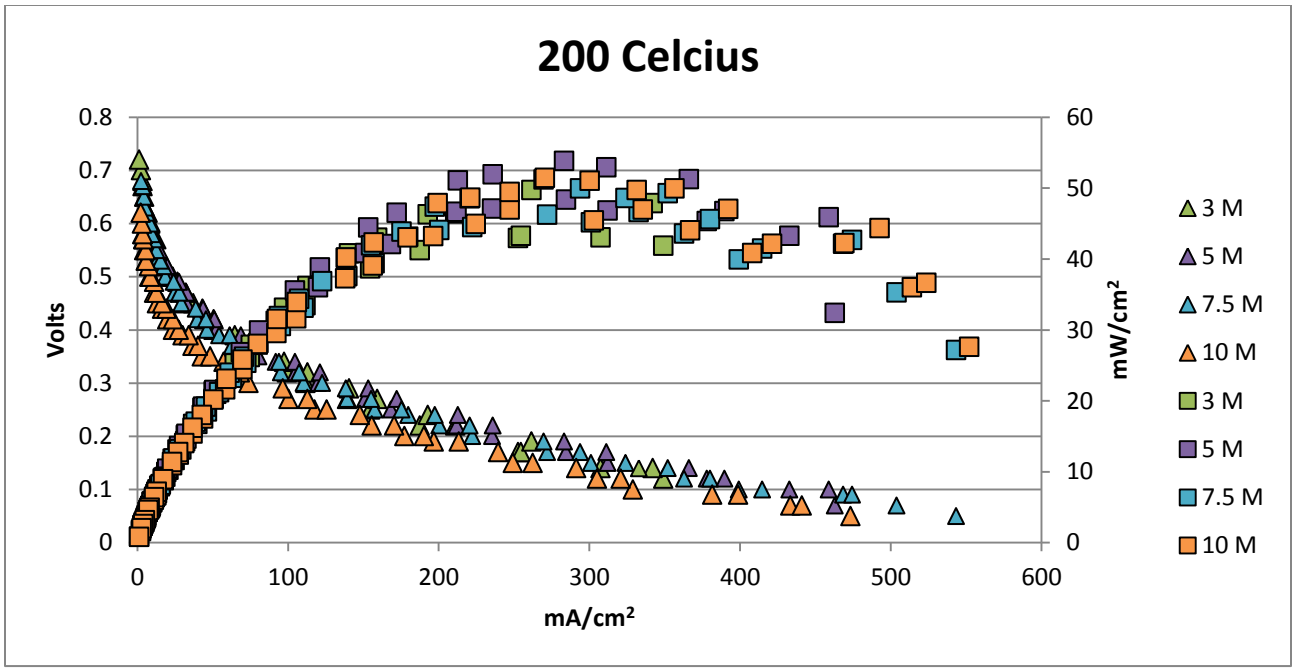

FIGURE 30: NORMAL AND EXPECTED RESPONSE WHEN COMPARING 3 M TO THE OTHER CONCENTRATIONS BY SHOWING ALL THE CONCENTRATION AT 200 C WITH THE PROPER FLOW RATE OF 1.5 ML/MIN.

As shown in the Figure 30, the 3M power density is almost indistinguishable from the others when it is at the same flow rate at 200˚C. There is some variation but the current density, and power density peaks are much lower than the other concentrations. Surprisingly, 5M had the highest value for mW/cm^2 while the 10M as predictably peaked at the highest value of current density, again indicating supply limitations. There is no significant difference at 200˚C between the higher concentrations of 5, 7.5 and 10M but 3M is still slightly below the others. Both the similarity among the higher concentrations and under performance of the 3M could be accounted for by the possibility of a lack of methanol available at the low concentration of 3M to fully interact with the MEA through the entire GDL layer. Overall however, there appears to be no significant difference in the concentrations of 5-10M at 200˚C for the direct methanol fuel cell. This is a very different result from that for conventional DMFCs

operating at much lower temperatures, when higher concentrations significantly surpass performance through a combination of cell poisoning and crossover.

Internal Reforming Layer Effect

After investigating the operating variable of temperature and concentrations, the cell's assembly was altered by adding a second anode gas diffusion layer and catalyst layer for investigating the effects of some internal reforming. The predominate reasoning behind this was to investigate whether this would eliminate the spread between data points at low voltages and provide higher performance. By allowing the methanol to react with the first outer anode, bringing more of the fuel reaction to completion. The test was performed at the standard temperature range specified by BASF of 160- 180˚C at concentration of 3, 5 and 10 M.

Throughout testing of the 3 M concentration illustrated in Figure 31 below it is easy to see that the internal reforming layer (DA) not only tightened the grouping as expected by reducing the oscillations but also increased the power and current densities. (This pattern also held true in both the 160 and 170˚C tests which can be seen in the Appendix.)

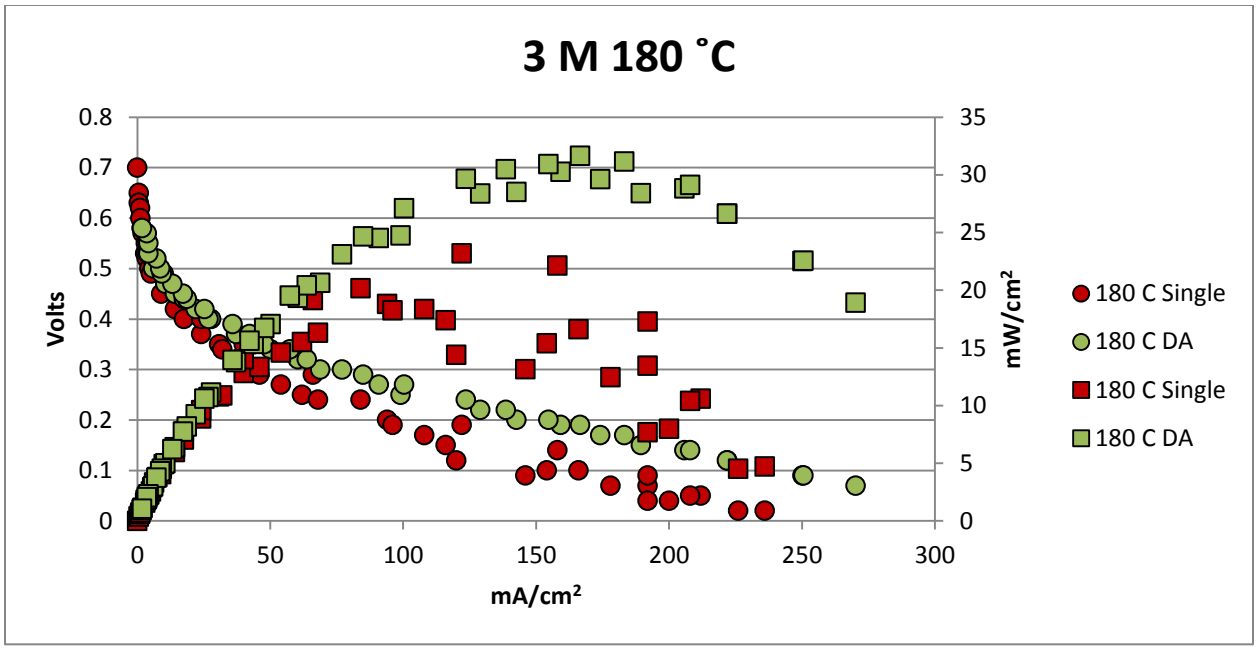

FIGURE 31: 3M METHANOL TESTS PERFORMED FIRST WITH A STOCK MEA (180 SINGLE) AND WITH AN ADDED ANODE GDL (180 DA) INTERNAL REFORMING

The overall spread of the readings decreased form a variation of over 30% to a maximum of below 10%. This was a drastic improvement as expected. The power density and current density increase, however, was surprisingly drastic, likely due to enhanced internal reforming. Additionally, the internal reforming layer may have allowed the methanol to fully utilize the full surface area of the cell due to an increase in diffusion resistance created by the double gas diffusion layer. By this reasoning, when the methanol entered the cell, it encountered a higher diffusion resistance to mass transfer in the GDL, and was thus forced to travel through the serpentine channels in the cell instead of moving straight through the gas diffusion layer to the catalyst thus utilizing a larger MEA area. Because the fuel would be more distributed over the cell, it would encounter more catalyst active area and would be able to react more completely as compared to the reaction with a single anode GDL. This reasoning is

supported by the evidence of the high temperature 3M tests mentioned earlier as with a single thickness anode side there was some evidence that the cell was not utilizing the total surface area provided by it due to a lack of methanol on the anode side at lower concentrations. When the MEA was inspected following testing with the standard setup, fouling was observed in about two channels, whereas the MEA showed fouling in five channels when a second anode GDL was added.

The 5 M tests with the internal reforming layer system were run under similar conditions to that of the 3 M, with the results for 180˚C shown below in Figure 32, and those at other temperatures placed in the Appendix.

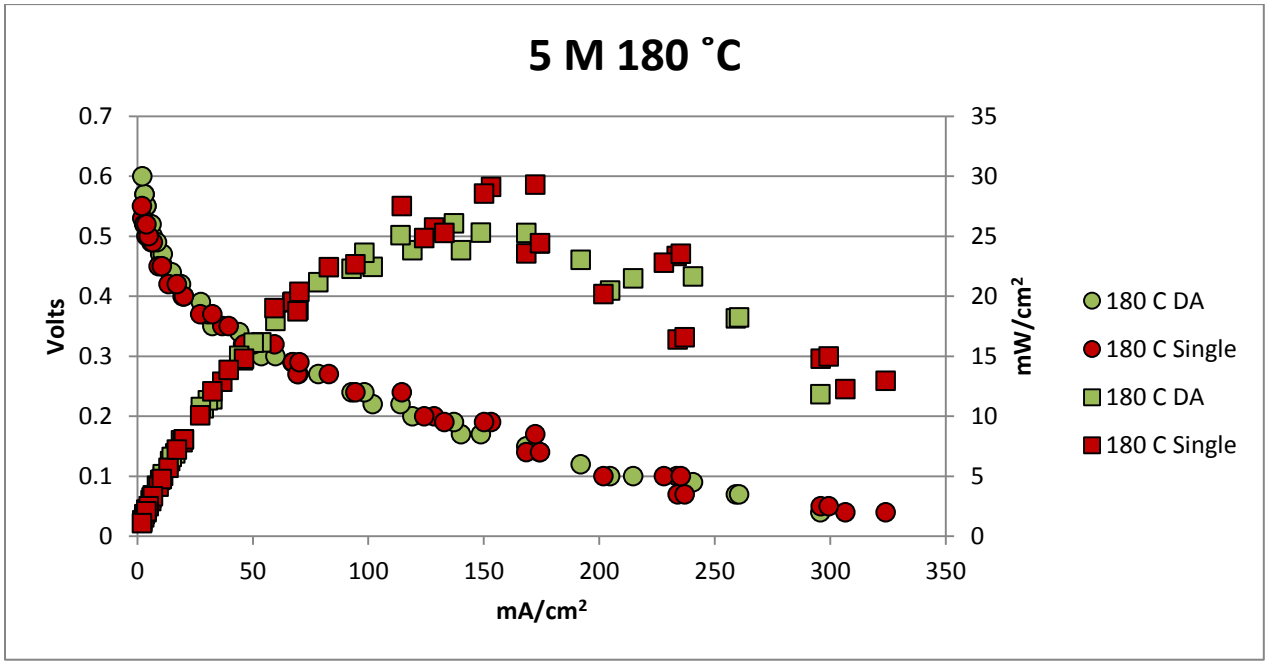

FIGURE 32: RESULTS OF 5M METHANOL TESTS AT 180˚C FOR SINGLE THICKNESS AND INTERNAL REFORMING LAYER

Unlike the 3M internal reforming layer testing, the 5M showed similar results for both the current densities and power densities. The spread for 5 M was however halved around the

peak current density, with no major differences in either current or power density maxima for the system.

The 10 M internal reforming layer was tested using the same conditions as the 3 and 5 M. The results of the 180˚C test are shown in Figure 33; the results of tests at other temperatures can be found in the Appendix, as the trends being studied were all repeated evenly across the three tested temperatures.

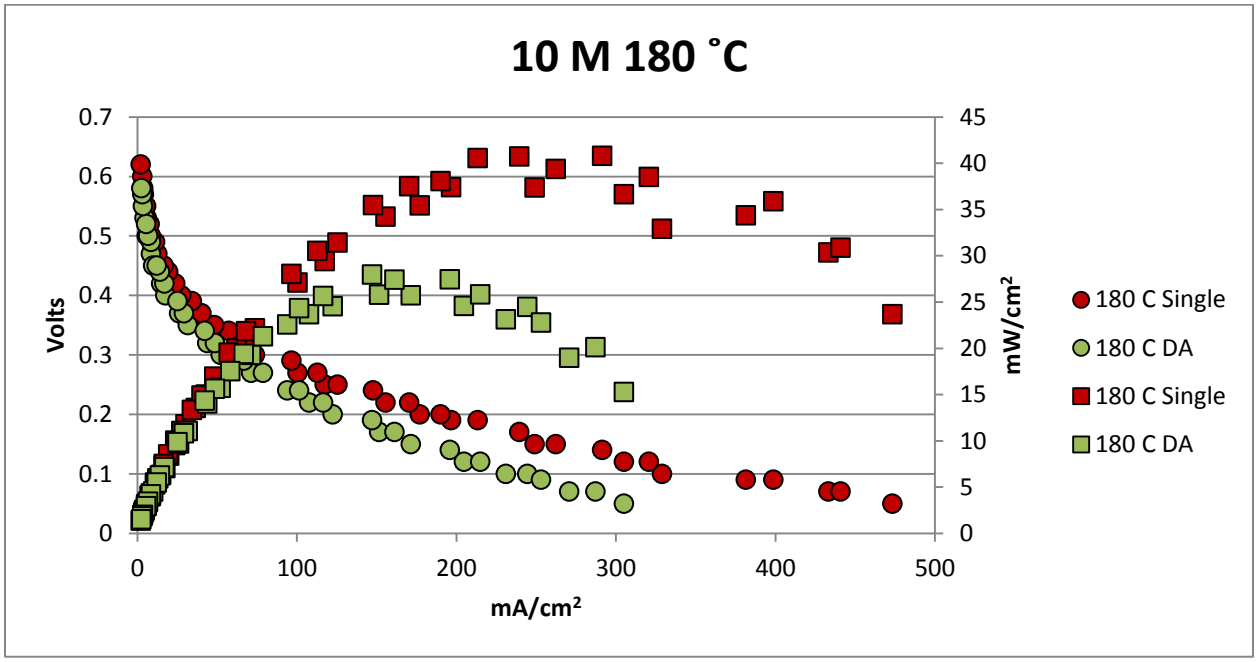

FIGURE 33: PLOT OF 10M METHANOL TESTS WITH AND WITHOUT AN INTERNAL REFORMING LAYER

The graph for 10 M tests displays the tightened grouping that was present with the other two concentrations. Unlike the other tests however, the 10M internal reforming layer showed a drastically diminished current and power density. It is possible that this is the result of higher diffusion resistance in the GDL. Alternatively it could be the result of possible degradation of the DA MEA.

Taking the whole collection of internal reforming layer test into consideration, the conclusions that can be drawn when analyzing the grouping patterns of the results illustrate that the pre-reactant internal reforming layer system provides a more consistent performance, however the effect on performance is not clear. It seems to have improved performance at the lower concentrations but reduced performance at the higher concentrations, the reasons for which are not clear.

By running a 10M internal reforming layer test at high temperatures it was found that the increase in performance of the DA layer was significant, as shown in Figure 34.

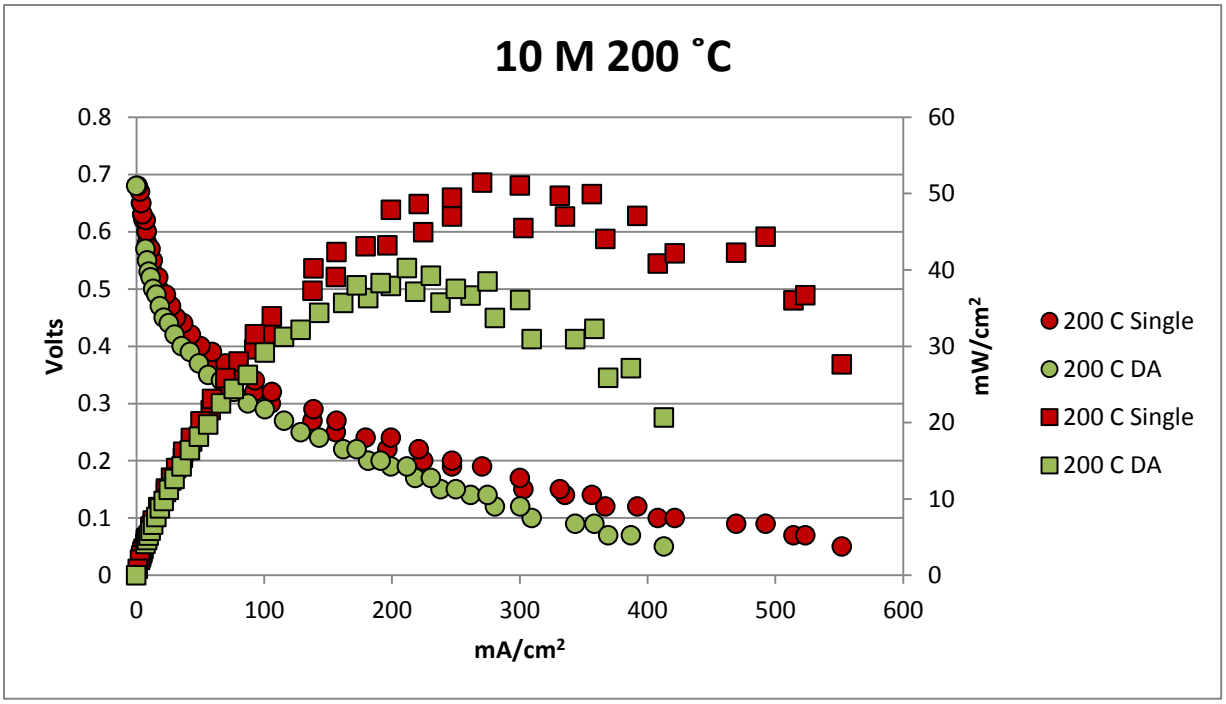

FIGURE 34: RESULTS FOR HIGH TEMPERATURE 10M INTERNAL REFORMING LAYER AT 200C

The results at 200˚C thus show that the internal reforming layer system's performance is increasing at a much larger rate than the single anode assembly in both power and current density. The single anode power density, for example, rose from a maximum of about 41

mW/cm ^{2} at 180˚ to about 51 at 200˚C. By contrast, the internal reforming layer power density increased from a maximum of about 28 mW/cm^2 at 180 to almost 40 mW/cm^2 at 200˚.

The maximum operating temperature tested for internal reforming layer was 220 at 10M and is plotted below against 10M 220 single anode testing.

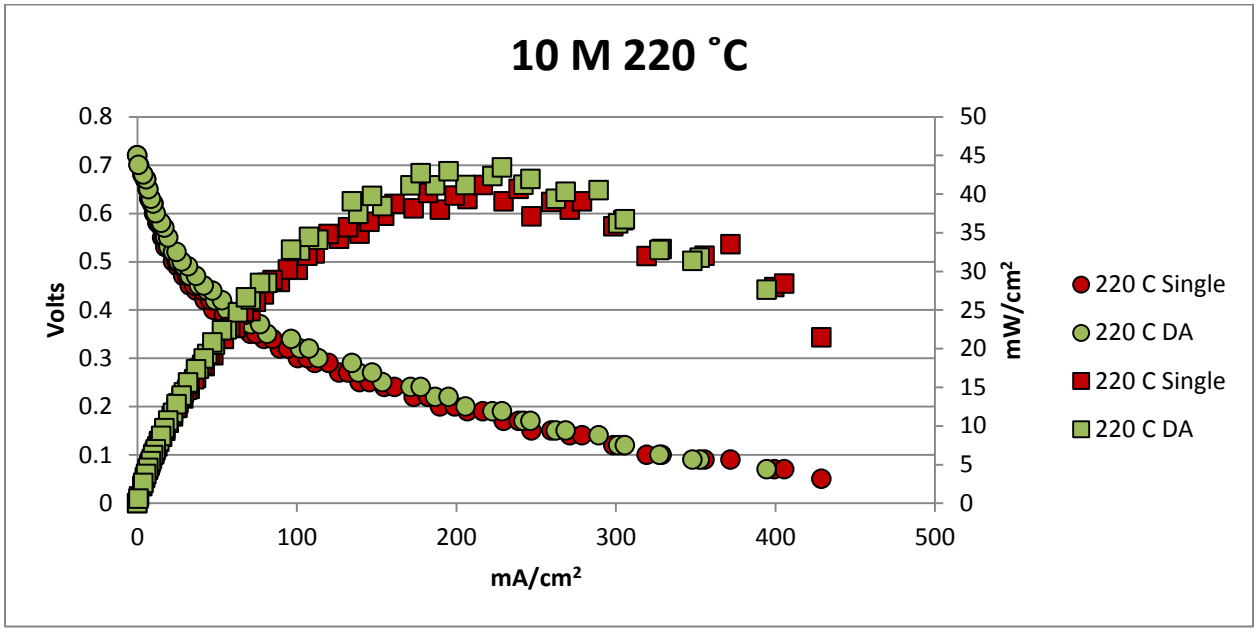

FIGURE 35: RESULTS OF 10M METHANOL TESTS AT 220˚C. SINGLE ANODE AND INTERNAL REFORMING LAYER CONDITIONS ARE COMPARED

As displayed in Figure 35, the double and single anode assemblies' power and current densities are around the same with the internal reforming layer slightly outperforming the single anode MEA. The internal reforming layer is also more consistent at higher amperage and produced a more consistent curve.

The matching densities at 220˚C which can be attributed to increased internal reforming kinetics from temperature increases indicates that the internal reforming layer may require a higher temperature to be fully effective. Additionally, the addition of the internal reforming

layer certainly aids in providing a consistent output, which would increase the predictability with which the cell is operated, making it safer for those operating the assembly.

Very High Concentrations

After completion of the internal reforming layer testing it was decided that still higher concentrations could be tested using the system. The first high concentration tested was neat (pure) methanol, which is 24.7 M, the results for which are shown in Figure 36.

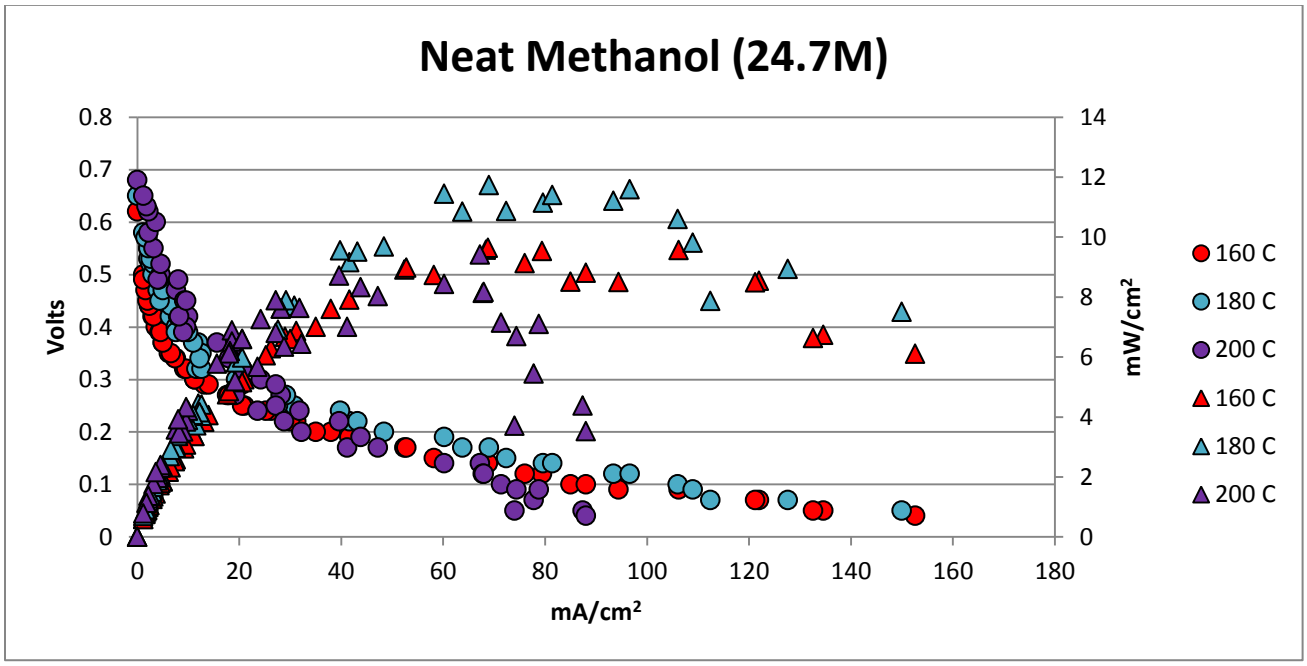

FIGURE 36: 24.7M METHANOL TESTED AT VARIOUS ELEVATED TEMPERATURES

As expected, the current densities increased with the increase in temperature up to 200 ˚C. However, at 200 ˚ the power density and current density drastically collapsed. Readings at all temperatures were erratic and the overall power and current densities were disappointing compared to the 10 M internal reforming layer that was run a few days before with the same apparatus shown below.

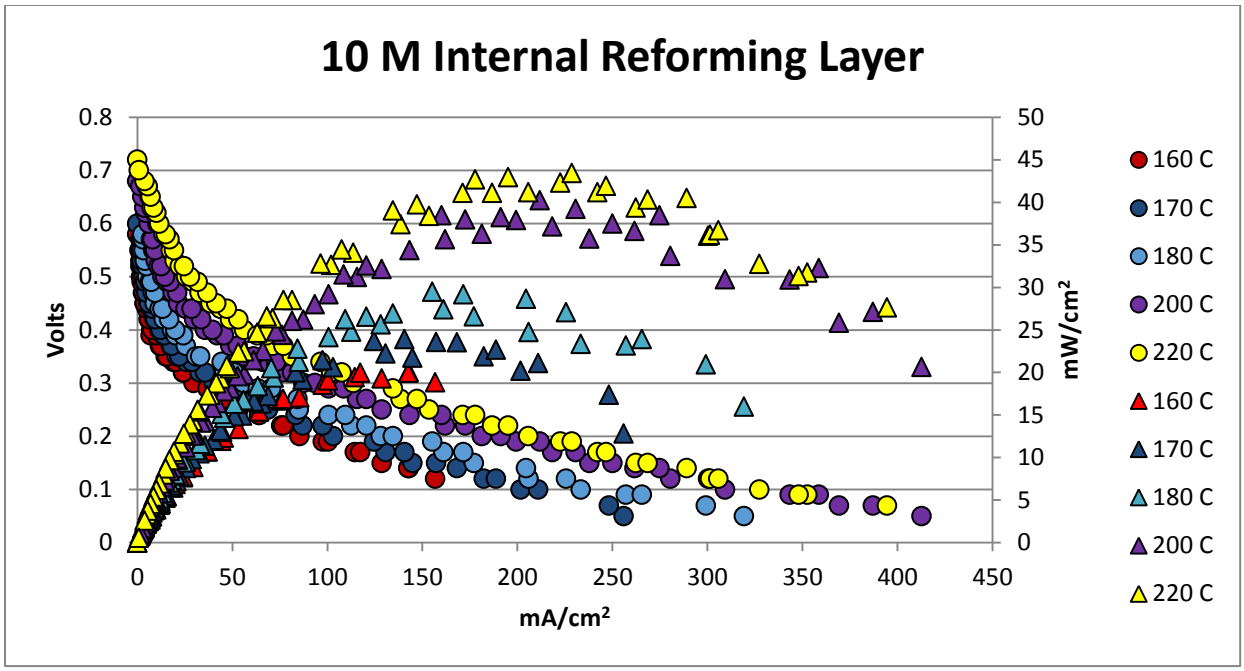

FIGURE 37: RESULTS OF 10M METHANOL TESTS AT ELEVATED TEMPERATURES

This is assumed to be a result of the lack of water in the system preventing the reaction required on the anode from occurring fully and thus limiting the cell's potential output. Recalling equation 6, the reaction of methanol at the anode requires the presence of water, which was not present in the pure methanol feed, although some water vapor is present as it is produced at the cathode. Based upon this equation, it was reasoned that there could potentially be an optimal region between 10 M and pure methanol. Thus, a 1:1 molar ratio between methanol and water was created to be tested (referred to as 17.1M for consistency). The results of this are shown below in Figure 38.

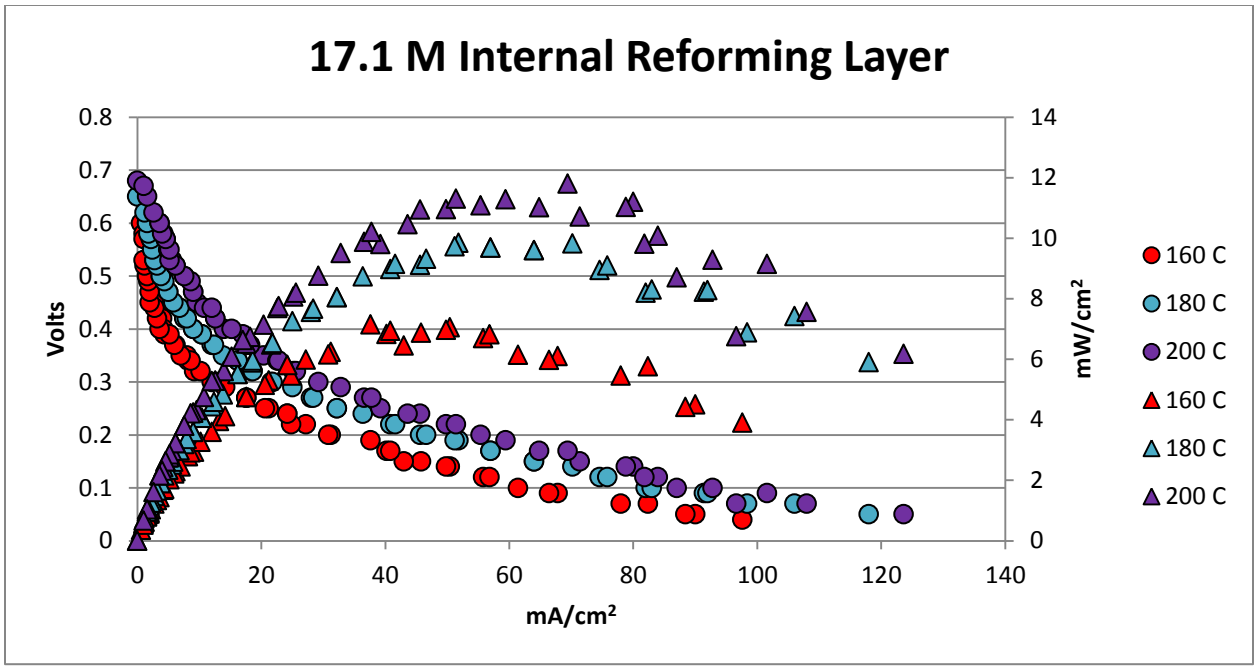

FIGURE 38: INTERNAL REFORMING LAYER TEST COMPLETED WITH 1:1 MOLAR RATIO OF WATER AND METHANOL

The results of the 17.1 M testing followed the kinetics expected and results from the temperature tests performed on the lower concentrations with increasing temperature producing both an increased power and current density. However, these values seemed low in comparison to the 10M results, and were similar to the low values of the 24.7 M tests. However, the results derived for 17.1 may not accurately reflect the effect of the concentration difference, but rather the result of damage to the cell from the pure methanol feed tests. A 10M baseline was run, thus, once more on the internal reforming layer cell yielding the following graph.

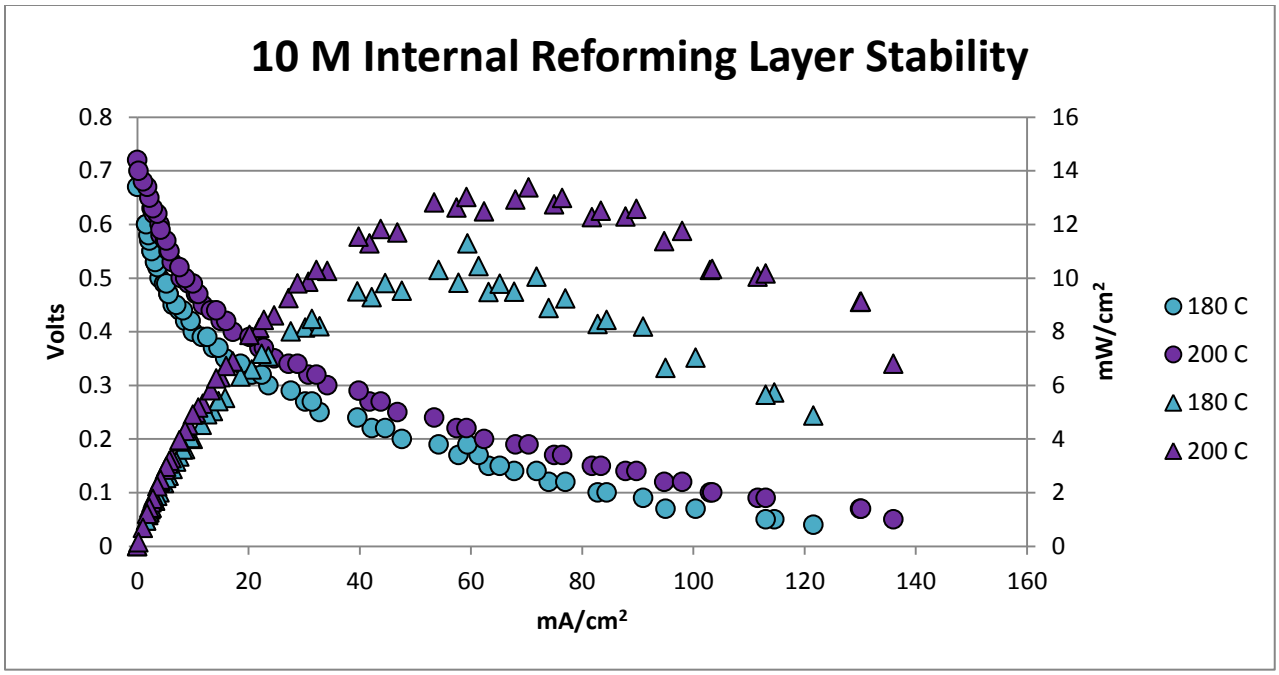

FIGURE 39: 10M METHANOL TEST PERFORMED TO CONFIRM DAMAGE FROM THE PURE METHANOL RUN

At 160 the cell was too variable to take readings and thus only 180 and 200 were able to be investigated. The low current and power densities indicate strongly that the cell was damaged and not operating at anything close to top conditions. The cell was disassembled and showed the same pattern that was seen after the 240˚C tests with 3 M with a white substance propagating through the channels on the anode, the result of damage to the MEA. From this it is theorized that running the cell at pure methanol (24.7M) caused damage to the MEA. A new MEA was thus loaded into the cell and activated fully before preforming a 10M baseline analysis the results of which are shown below.

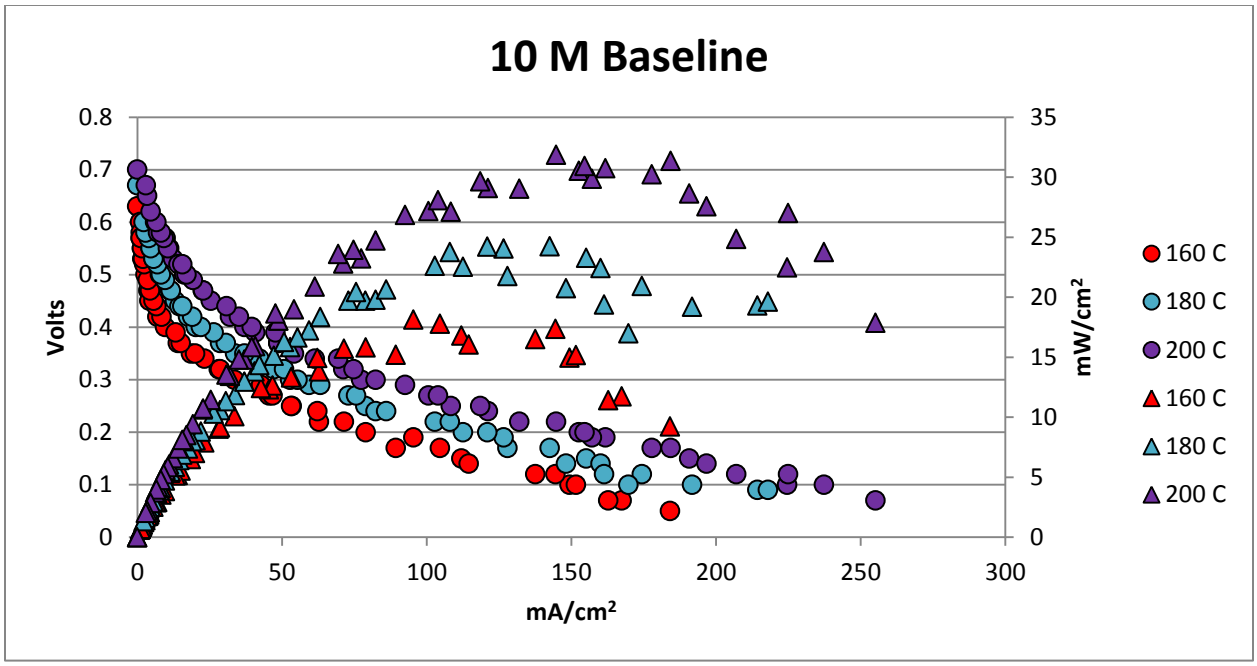

FIGURE 40: NEW TEST SHOWING THE RESULTS OF VARIOUS TEMPERATURES. THIS TEST WAS PERFORMED IN ORDER TO PROVIDE A COMPARABLE DATA TO A NEW MEA.

The cell's overall trends match what was expected for a new MEA although values were slightly lower than before. This was most likely due to the variability between MEA's within a set. It was decided that while another 17.1 molar test would not be comparable to any of the other tests due to the low MEA performance, it could be compared to this 10M baseline. This would indicate whether the desired optimal concentration was in the range of 10-17.1M, or from 17.1-24.7M, as a lower performance at 17.1 would indicate the optimum was closer to 10M and a better performance would indicate the optimum was closer to 24.7M. The graph below displays the results of the single anode 17.1M test.

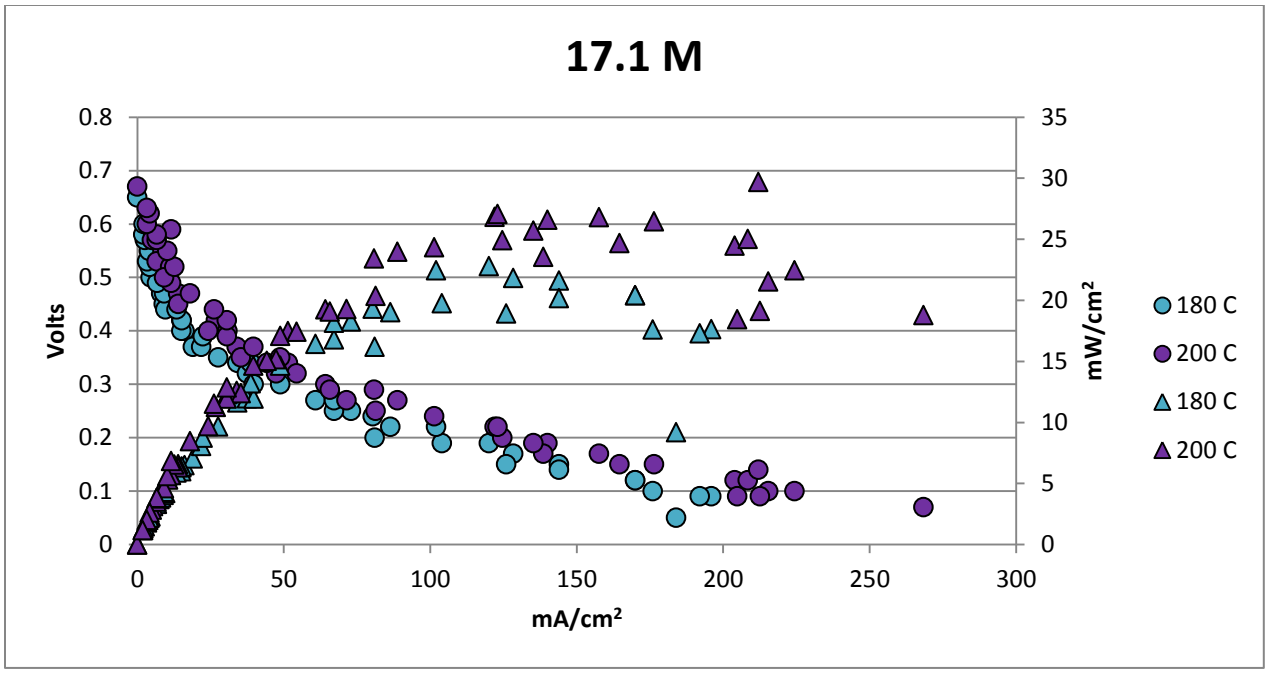

FIGURE 41: RESULTS OF TESTS PERFORMED TO ESTABLISH HIGH-CONCENTRATION TRENDS.

While collecting the data, the cell acted erratically providing lower amperages at lower voltages (all previous test showed increased amperage with decreased voltage). Additionally, the temperature of the feed line indicating the inlet methanol temperature fluctuated rapidly possibly skewing the data. The data that was collected however shows a slightly diminished performance compared to the 10M tests that were run (Figure 40) which is the only comparable graph from the same MEA. This would indicate that the optimum concentrations of methanol for the system is between the two concentration of 10M and 17.1M.

Open Current Voltages

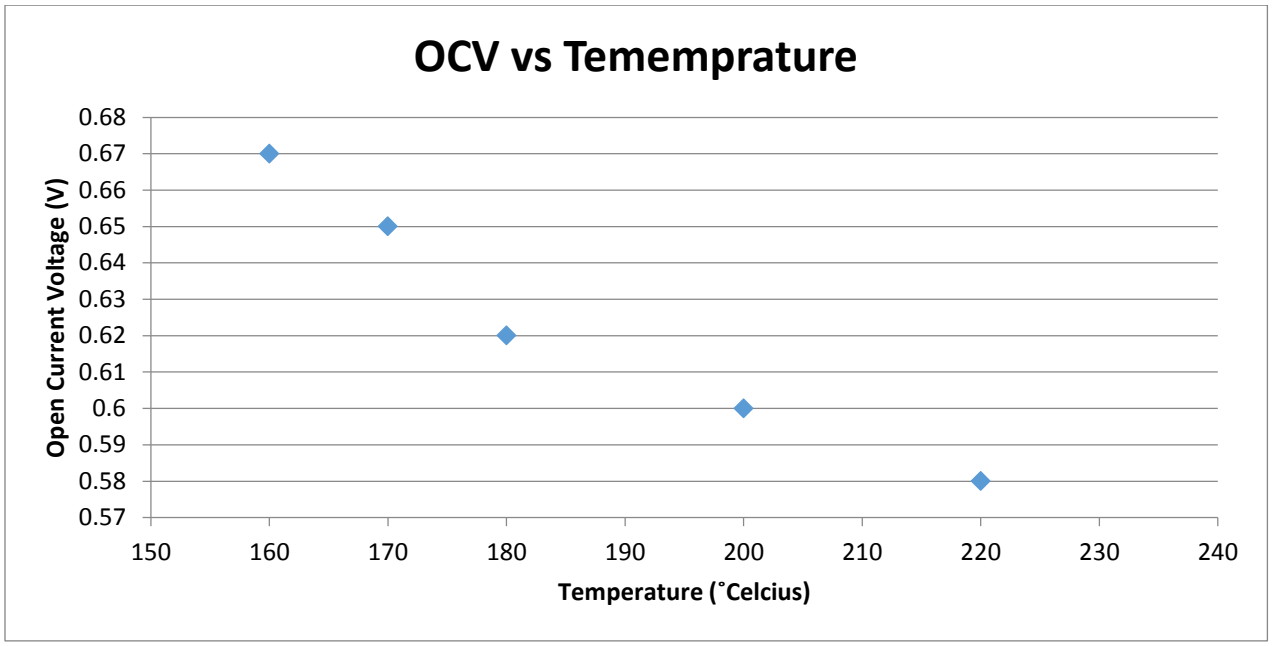

FIGURE 42: OPEN CURRENT VOLTAGES FOR 10M

Finally, the open current voltages for a 10M feed are plotted in Figure 42 and are found to decreased with an increase in temperature. This is a result of the increased crossover at higher temperatures. This plot serves as a validation that we have a good understanding of how to predict the performance of the cell, and shows that the cell is operating in a manner which conforms to the norms of operation observed for other fuel cells regardless of fuel makeup and specific materials of construction.

5. Conclusions and Recommendations

After completing the investigation and reviewing the analysis of the data, an overall "optimal operating conditions" appear to depend on the cost and safety of the system. The largest impact on the system was clearly the temperature which increased kinetics and lead to the greatest improvement in performance. The improvement in kinetics at 200˚C was so strong that the molarity of the feed had a minimal effect. The largest effect of molarity came with at lower operating temperatures where the differences can be easily seen between the spread in increasing concentration at 180 and the tight grouping of concentrations at 200 ˚C. This indicates that the effects of concentration are heavily dependent on the temperature and in the development of an efficient methanol fuel cell for commercial use the optimal feed would depend upon the highest operating temperature possible from a durability standpoint, which was not investigated here.

Originally PBI DA was not thought to be feasible because of issues of phosphoric acid leaching that arose from operation with a liquid methanol feed. This was overcome via heating to vaporize feed, which provided results similar to other conventional methanol fuel cells which operate at around 50 mW/cm^2 at peak current density. Furthermore, in comparison to standard low temperature direct methanol fuel cells, only one quarter of the catalyst was used to produce the same electrical output. Therefore, further research into PBI DA-based MEAs is not only feasible, but warranted. Further, it could handle much higher concentrations of methanol, as opposed to the 1M standard for lower temperature DMFCs.

Throughout the development of this project, certain parameter changes were discussed which may have yielded interesting results when implemented, but because of technical and

time constraints, their investigation was not feasible. Here are reported possible suggestion for future investigation of the high temperature DMFC to improve the understanding of the system.

One area which deserves added attention is the way in which the alcohol feed is converted from its liquid state to the vapor. In this work, the methanol feed was brought to a boil in a furnace and pumped as a vapor to the inlet of the apparatus. We believe interesting results may be found through investigating an alternative means of transporting the fuel, namely via bubbling with nitrogen feed through a liquid feed reservoir. We conceived, but never implemented an apparatus that would draw a stream of nitrogen (or another inert) through a vessel containing pure methanol or a methanol-water mixture. In this way the inert would transport the methanol vapor (in a concentration equal to the vapor pressure of the feed at the specified temperature) without the need for extensive heating to boil the alcohol and the possibility of condensation in the lines. In this case, care would have to be taken to ensure that only evaporated methanol is able to enter the cell. If any liquid is transported to the cell without being evaporated, it will strip the acid from the MEA and cause permanent damage to the catalyst and PEM, as we found in this study.

In the course of this work, we also investigated the possibility of using ethanol as the fuel fed to the cell. Because of the constraints, this aspect of operation was never fully investigated, and it would be our recommendation that the full potential of ethanol feed be explored at high temperatures in a fuel cell. In our investigations, we ran ethanol in the system and observed fair results; however when the system was reverted to running on methanol, the output was improved compared to our initial methanol results. It is unclear if this improved

performance is a result of priming the MEA with ethanol or if other factors were at play, so an in-depth study of this condition may prove fruitful. It has been suggested that ethanol will oxidize to acetic acid in a direct ethanol fuel cell, which may help the proton exchange characteristics and more efficiently facilitate the oxygen reduction kinetics (Kim, et al., 2011). The tests that were conducted with ethanol only produced a current density of 120 mA/cm^2 and power density of 20 mW/cm^2 at 170 ˚C and only showed an improvement to a current density of150 mA/cm^2 and power density of 22 mW/cm^2 at 180 ˚C. Compared to the methanol testing done, these results indicated that either the cell had issues with processing ethanol or there is another factor that influenced the low results. Further testing would have to be done in order to produce a reliable correlation between performance and ethanol.

While taking the data that make up this report, we observed significant error in reading voltages and amperages from the load box. Especially at high current densities, the readings would fluctuate and an average or representative value would have to be chosen for the data analysis. It is known that oscillation of current can take place in a cell because of the successive fouling and clearing of carbon monoxide from the catalyst layer. This may contribute to the uncertainty in our readings, so we believe an investigation into the full extent of this variability is warranted. Our data were taken approximately ten seconds after an electronic parameter was changed. We determined that this was enough time to establish representative performance based on recommendations from our predecessor. Future experimentation could look into the pattern of oscillation which will be observed over a longer time span (say, a few minutes at each voltage setting), which could serve to validate method for data collection.

This report summarizes a series of tests done at temperatures above what is recommended by the manufacturer, BASF. In these tests performance did not seem to be compromised by operating outside of the recommended range. It seems that the temperature range provided does not constitute the only range in which the cell is operable, but it may describe a range outside of which long term use is damaging to the apparatus. We would recommend that an investigation be conducted to investigate the long term effects of operating the cell at temperatures above 180˚C. Our tests constituted a timespan of about four hours during which the cell was at an elevated temperature. When operated at these conditions for longer, we may see performance loss resulting from thermal damage to the catalyst, or from the phosphoric acid drying from the PBI membrane.

In executing the experiments described above, the parameter of fuel flowrate was never changed from its initial value of 1.5 mL/min. Possible future work could be conducted to establish the role of feed flowrate in potentially improving the results seen at the various concentrations. It has been shown here that running the cell at too-high concentrations of methanol has negative effects on the performance of future tests. It is theorized that this occurs because of over-population of the catalyst layer with methanol without sufficient water to facilitate proton transfer mechanisms. Because of the one-to-one stoichiometry of water and methanol in the reaction of the cell, the optimal theoretical concentration of methanol is 17.1M, which constitutes a one-to-one stoichiometry in solution. This report shows lower-than-expected performance under this condition, so it would be recommended that future work focus on applying this concentration of solution at lower flowrate to see if it can be implemented without ruining the performance with too much methanol.

Finally, we recommend that a systematic investigation be conducted of the performance of the high temperature DMFC with air as the cathode feed, which is of practical interest, rather than with pure oxygen, as used here.

6. Works Cited

Agmon Noam The Grotthuss mechanism [Journal] // Chemical Physics Letters. - 1995. - Vol. 244. - pp. 456-462.

Andujar J.M. and Segura F. Fuel cells: History and updating. A walk along two centuries [Journal] // Renewable and Sustainable Energy Reviews. - 2009. - Vol. 13. - pp. 2309-2322.

Avgouroloulos G. and Neophytides S. G. Performance of internal reforming methanol fuel cell under various methanol/water concentrations [Journal] // Journal of Applied Electrochemistry. - 2012. - Vol. 42. - pp. 719-726.

Barczuk Piotr J. [et al.] Enhancement of catalytic activity of platinum-based nanoparticles towards [Journal] // Journal of Power Sources. - 2010. - Vol. 195. - pp. 2507-2513.

Cho Y. [et al.] The Imporved Methanol Tolerance Using Pt/C in Cathode of Direct Methanol Fuel Cell [Journal] // Electrochemica acts. - 2008. - Vol. 53. - p. 5909.

Colon-Mercado Hector R. and Popov Branko N. Stability of platinum based alloy cathode catalysts in PEM fuel cells [Journal] // Journal of Power Sources. - 2006. - Vol. 155. - pp. 253-263.

Datta Ravindra Background Notes [Interview]. - Worcester : [s.n.], April 17, 2014.

Datta Ravindra Fuel Cell Basics [Interview]. - February 25, 2014.

Datta Ravindra Meeting Minutes through April 18 2014 [Interview]. - March 3, 2014.

Datta Ravindra The Essential Fuel Cell Model [Interview]. - March 3, 2014.

Do Samantha, Spetka Kaitlyn and Suarez Matthew The Effect of Temperature on the Performance of Direct Methanol Fuel Cells [Report]. - Worcester : Worcester Polytechnic Institute, 2012.

DuPont Fuel Cells Safe Handling and Use of Perfluorosulfonic Acid Products [Online] // fuelcells.dupont.com. - 2009. - Arpil 19, 2014. - http://www2.dupont.com/FuelCells/en_US/assets/downloads/dfc301.pdf.

Fogler H. Scott Elements of Chemical Reaction Engineering [Book]. - [s.l.] : Prentice Hall, 2005. - 4.

Giner Inc. Direct Methanol Fuel Cells (DMFC) [Online] // ginerinc.com. - March 18, 2014. - http://ginerinc.com/products.php?a=DMFC.

Gubler Lorenz [et al.] Celtec-V: A Polybenzimidazole-Based Membrane for the Direct Methanol Fuel Cell [Journal] // Journal of The Electrochemical Society. - 2007. - pp. B981-B987.

Hadfield Chris An Astronaut's Guide to Life on Earth [Book]. - Toronto : Vintage Canada, 2014.

Henschel Carsten Cell Assembling and Start-up Proceedure for Celtec P-MEA. - Ludwigshafen : [s.n.], March 2012.

Henschel Carsten Delivery of Celtec MEAs [Interview]. - February 21, 2014.

Henschel Carsten Delivery of Celtec MEAs [Interview]. - 2014.

Institute for Energy Research Energy Overview [Online] // Institute for Energy Research. - 2014. - April 20, 2014. - http://www.instituteforenergyresearch.org/energy-overview/fossil-fuels/.

International Energy Agency World Energy Outlook 2013 [Book]. - [s.l.] : OECD Publishing, 2013.

Israni S. H. and Harold M. P. Methanol Steam Reforming in Single-Fiber Packed Bed Pd-Ag Membrane Reactor: Experiments and Modeling [Journal]. - [s.l.] : Journal of Membrane Science, 2011. - Vol. 369. - pp. 375-387.

Kamarudin K.Z.F. [et al.] Review: Direct ethanol fuel cells [Journal] // International Journal of Hydrogen Energy / ed. 38. - 2013. - pp. 9438-9453.

Kang Segoo [et al.] Stability and durability of PtRu catalysts supported on carbon [Journal] // International Journal of Hydrogen Energy. - 2012. - Vol. 37. - pp. 4685-4693.

Kim In [et al.] Catalytic Reactions in Direct Ethanol Fuel Cells [Journal] // Angewandte Chemie International Edition. - February 8, 2011. - 10 : Vol. 50. - pp. 2270-2274.

Kim In [et al.] Catalytic Reactions in Direct Ethanol Fuel Cells [Journal] // Angewandte Chemie International Edition. - 2011. - Vol. 50. - pp. 2270-2274.

Kreuer K. D., Rabenau A. and Weppner W. Vehicle Mechanism, A New Model for the Interpretation of the Conductivity of Fast Proton Conductors [Journal]. - [s.l.] : Angew. Chem. Int. Ed. Engl., 1982. - Vol. 21. - pp. 208-209.

Liang Z., Zhao T. and Xu J. Stabilization of the platinum-ruthenium electrocatalyst against the dissolution of ruthenium with the incorporation of gold. [Journal] // Journal of Power Sources. - 2008. - pp. 166-170.

Liu H. and Zhang J. Electrocatalysis of Direct Methanol Fuel Cells: from Fundamentals to Applications [Book]. - Darmstadt, Germany : Wiley-VCH, 2009.

Liu Jianguo [et al.] Effects of methanol concentration on passive DMFC performance [Journal]. - [s.l.] : Fuel Cell Bulletin, 2005. - 2 : Vol. 2005. - pp. 12-17.

Miessler Gary L. and Tarr Donald A. Inorganic Chemistry [Book]. - Upper Saddle River : Pearson Educational, Inc., 2011. - 4.

Modestov A.D. [et al.] Degradation of high temperature MEA with PBI-H3PO4 membrane in a life test [Journal] // Electronica Acta. - 2009. - Vol. 54. - pp. 7121-7127.

Nandanwar S.U. [et al.] Stability of ruthenium nanoparticles synthesized by solvothermal [Journal] // Crystal Research and Technology. - 2011. - 4 : Vol. 46. - pp. 393-399.

O'Hayre R. [et al.] Fuel Cell Fundamentals [Book]. - Hoboken : John Wiley & Sons, 2009.

Ohtake Toshidito and Mori Tohru, Morikawam Yutaka Catalytic Conversion of Methanol by Oxidative Dehydrogenation [Journal] // Journal of Natural Gas Chemistry. - 2007. - Vol. 16. - pp. 1-5.

Ortiz-Rivera Eduardo, Reyes-Hernandez Angel L. and Febo Rey A. Understanding the History of Fuel Cells [Journal] // 2007 IEEE Conference on the History of Electric Power. - 2007. - pp. 117-122.

Park Young-Chul [et al.] Design of a MEA with multi-layer electrodes for high [Journal] // International Journal of Hydrogen Energy. - 2012. - Vol. 37. - pp. 4717-4727.

Pivovar Bryan Scott [et al.] Methanol Crossover in Direct Methanol Fuel Cell Systems [Conference] // 2003 Meeting of the Electrochemical Society. - Paris : [s.n.], 2003.

Schuster M [et al.] [Journal] // Fuel Cells. - 2005. - Vol. 5. - p. 355.

Smithsonian Institution Fuel Cell Origins [Online] // AmericanHistory. - 2004. - April 17, 2014. - http://americanhistory.si.edu/fuelcells/origins/orig1.htm.

Tijm P.J.A, Waller F.J. and Brown D.M. Methanol technology developments for the new millennium [Journal] // Applied Catalysis A, General. - 2001. - Vol. 221. - pp. 275-282.

Wang Guoxiong [et al.] Effect of carbon black additive in Pt black cathode catalyst layer on direct methanol fuel cell performance [Journal] // International Journal of Hydrogen Energy. - 2010. - pp. 11245-11253.

Wiese W, Emonts B and Peters R Methanol Steam Reforming in a Fuel Cell Drive System [Journal]. - [s.l.] : Journal of Power Sources, 1999. - Vol. 84. - pp. 187-193.

XCellsis Module 1: Hydrogen properties [Article] // Hydrogen Fuel Cell Engines. - [s.l.] : XCellsis, Ballard, Fedral Transit Administration, Advance Transportation Technology, 2001.

Zurowski Artur [et al.] Activation of carbon-supported platinum nanoparticles by zeolite-type cesium [Journal] // Journal of Electroanalytical Chemistry. - 2010. - pp. 238-247.

Appendix A: Acronym List

˚C	Degrees Celsius
180N	180 New MEA
A	Pre-exponiential Factor used in the Arrhenius Equation
BASF	Badische Anilin- und Soda-Fabrik
CH2OH	Hydroxymethyl
CHOH	Methanol Ion
cm2	Centimeter Squared
CO	Carbon Monoxide
CO2	Carbon Dioxide
COH	Aldehyde
COOH	Carboxylic
DA	Internal reforming layer (Double Anode Thickness)
DMFC	Direct Methanol Fuel Cell
E	Activation Energy
e-	Electron
F	Flouride Atom
GDL	Gas Difusion Layer
H	Hydrogen Atom
H2	Hydrogen
H2O	Water
H3O	Hydronium
HCOOH	Formic Acid
K(t)	Rate Constant
mA	milli Amperes
mA/cm2	Current Density
MEA	Membrane Electrode Assembly
mW	milli Watts
mW/cm2	Power Density
η_d	Overpotential of diffusional factors
η_{EL}	Ohmic potential drop from conduction of ions
η_I	Overpotential of interfacial resistance
η_k	Overpotential of kinetic processes
η_x	Overpotential of fuel crossover
η_A	Overpotential at the anode
η_C	Overpotential at the cathode
$\phi_{C,O}$	Potential at the cathode
$\phi_{A,O}$	Potential at the anode
O2	Oxygen

OCV	Open Current Voltage
PBI	polybenzimidazole
R	Gas Constant
S	Side Group
SO3H	Sulfonic Acid
T	Temperature (Kelvin)
V	Volts
W	Watts

Appendix B: Operating Instructions

Syringe Pump

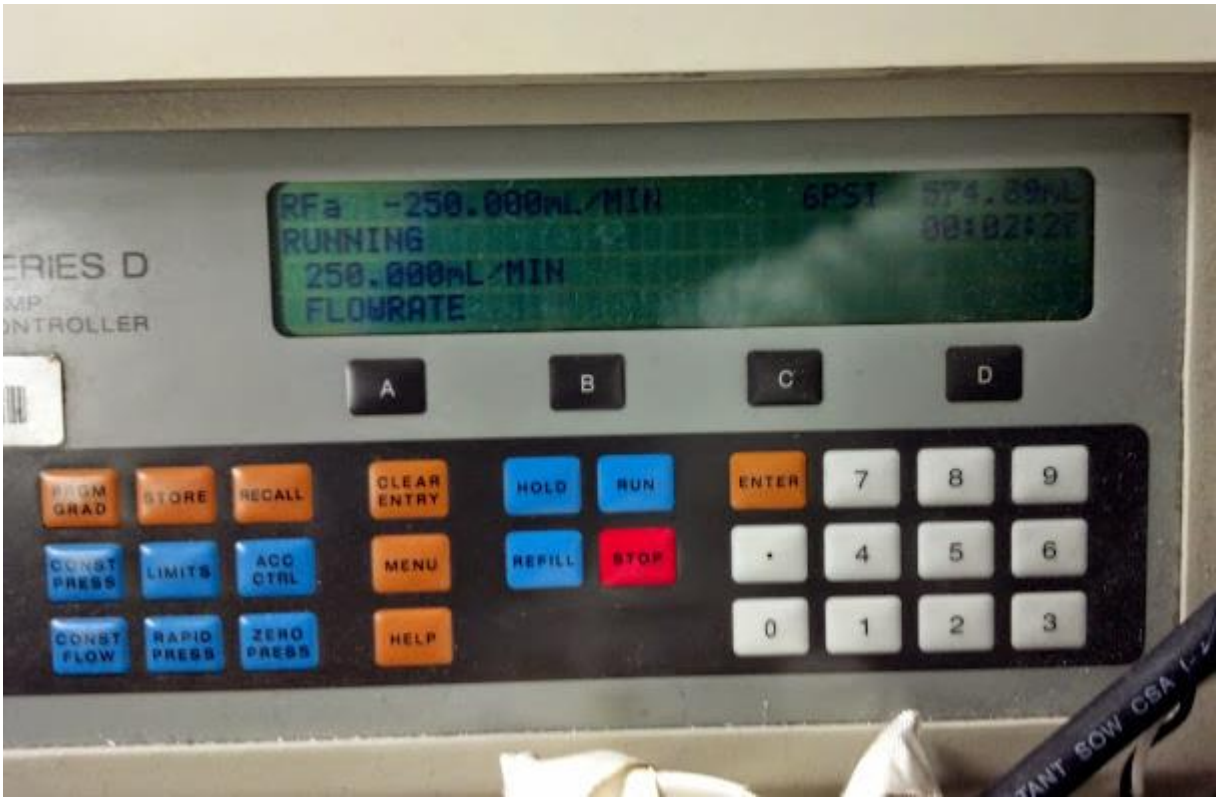

FIGURE 43: SYRINGE PUMP PANEL

1. Turn on power to the pump by activating the switch first on the pump itself, then on the control box.
2. Remove tubing connection to furnace and place the line in a collection vessel
3. Adjust the flowrate of the pump by pressing “A” and entering the numerical value of the desired milliliters per minute on the number pad; press “Enter.”
4. Press “Run” to activate flow from pump into the collection vessel
5. When the pump has emptied (as displayed on the control readout) remove the tubing from the collection vessel and place it in the container with the liquid to be loaded to the pump.

6. Press “Refill” to begin filling the pump (again, use the number pad to specify the flowrate).
7. When the pump reads as full, wait a few minutes for the pressure in the pump to stabilize (this ensures that the pump has taken in all the liquid it can)
8. Turn the pump to Run mode until some liquid flows into the vessel, stop the pump and reconnect the line to the furnace
9. Set the desired flowrate and press “Run” to start the flow from the pump to the furnace and the cell.

Hints for Use

1. Visually check the flowrate setting before running the pump as it can revert to a previous setting between refilling and running.
2. After filling the pump, running at a higher flowrate (around 15 mL/min) will ensure that the line has no air left in it.
3. Though the pump will usually have a pressure of less than 20 psi, one must be careful to keep the pressure below 30psi for the health of the pump.
4. When the pump is to be left for more than a day between tests, it should be emptied of alcohol and filled with deionized water. Also, then transitioning from one alcohol concentration to another, fill the pump with DI water between the alcohol concentrations to ensure that the proper concentration is achieved in the pump

Temperature Controlers

FIGURE 44: TEMPERATURE CONTROL BOXES

The three temperature control boxes built into the station control the furnace, the cell and the feed line (left, center, and right respectively). The boxes are connected to the heating tape throughout the apparatus, and the thermocouples located in the furnace, cell and feed line. The heating tape is only capable of providing energy to the various parts of the apparatus, and cannot cool the system. Cooling must be done by free convection with the atmosphere. Because of this, it is important to ensure that the components are not allowed to reach temperatures which are dangerous for the apparatus because cooling can take several hours. Because of the control parameters in the control units, the temperature in the furnace can overshoot the set point by up to a few dozen degrees, but the cell will not be allowed to heat beyond the set point as this is the most sensitive part of the apparatus. Because of the tuning parameters in each control, the furnace will be brought above its set point within minutes of a servo-mechanism set point change, while it will take the cell about fifteen minutes to establish a 10˚C change. It must be noted that the heating elements run from power provided by the power strip located at the back of the apparatus. It is also imperative to keep the thermocouples in place in the furnace, feedline and cell. If the control boxes are used without

the thermocouples in place, they will constantly read a high set point offset and will continue to apply heat.

Load Box

FIGURE 45: LOAD BOX

1. When there is flow of oxygen and fuel, turn external power to load box on using toggle switch on front.
2. To specify the amperage of the cell (and allow voltage to fluctuate naturally) select “Mode” then “Curr.” To specify voltage select “Mode” and “Volt). To specify Ohms, select “Mode” and “Res.”
3. Enter the desired parameter value using the number pad and press “Enter” to finalize selection. The ← button can be used to undo the last number entry if an error is made.
4. Alternatively, the parameter can be changed by small increments by pressing the “Input↑” or “Input↓” button.

   Note: When first changing the parameter which is to be held constant, the load box may assign an initial value to this parameter. This can be a dangerous value, as it has been observed that

the voltage default value is 60V, whereas a value of 0.7V is usually desirable. In cases like this it is important to manually change the input quickly to avoid damage to the cell.

Methanol Feed

1. Once the cell, feed line and furnace are heated (at lease to 100˚C to prevent liquid water formation), ensure that the pump is filled with enough methanol.
2. Run the pump while the line is on bypass until methanol is observed past the feed juncture.
3. When the line is charged with methanol, stop the flow using the pump controls.
4. Stop the flow of nitrogen using the needle valve located on the flow controller on the tank regulator.
5. Remove the nitrogen line from the anode inlet, and replace it with the methanol line just after the three-way junction connected to the feed pressure gage. Tighten with a 7/16ths wrench until slight resistance.
6. Once the oxygen line is also connected, turn on the load box and begin testing.

Hydrogen/Oxygen Feed

1. Once the cell, feed line and furnace are at temperature, stop the feed of nitrogen using the needle valve on the gas tank regulator.
2. Ensure that the flow of hydrogen and oxygen is pressurized up to the needle valve. This is done by fully closing the needle valve (clockwise turn) and turning the release valve on the tank itself to the Open position until a pressure reads on the upstream gage.

3. Disconnect the nitrogen lines from the cell using the 7/16ths inch wrench, and quickly replace with the appropriate gas flow (hydrogen on the anode for an activation run, and oxygen on the cathode for any test where reactions in the cell are desired).
4. Slowly turn the needle valve on the appropriate tank regulator (starting with hydrogen if needed) until 1-2psi is displayed on the gages. Be sure to balance the pressures, as a differential of 5psi will cause damage to the MEA.
5. When pressure is regulated, turn on the load box to allow the reactions to begin. Do not turn on the load box until both gases (or oxygen and methanol) are flowing, or the application of current will strip elections from the MEA instead of the fuel.

Nitrogen Feed

1. To attach the nitrogen, it may be necessary to remove the lines of methanol and oxygen if a test has been underway. Do this using a wrench, and try to minimize the time during which the cell is not connected to any gas line between tests or activation can be compromised.
2. Ensure that the nitrogen tank regulator is charged up to the needle valve. Turn off the needle valve and turn on the flow directly from the tank until a pressure is registered on the upstream gage of the regulator.
3. Once the lines are connected to both sides of the cell, slowly turn the needle valve to apply pressure to the line. Regardless of differential the total pressure in the cell should not exceed about 5psi.

Replacing the MEA

1. After the final test, the cell should be allowed to cool overnight before it is disassembled because the graphite plates have a high specific heat, and will stay hot for up to several hours past the final application of heat from the heating tape.
2. Remove the gas lines from the anode and cathode using the wrench.
3. Remove the waste lines.
4. Remove the thermocouple.
5. Unplug the heating elements from the power outlet behind the apparatus.
6. Move the cell from the insulating plate to a more open lab bench.
7. Remove the screws in a star pattern (i.e. one screw from the top, bottom, left and right sides of the cell, then repeat until all screws are removed).
8. Carefully remove one plate from the other. The MEA and gaskets are held in place with a pair of ceramic dowels. These have a tendency to stick, so make sure the MEA is secured to one plate so that it is not torn during disassembly.
9. Use a paperclip or thumbtack to clean any obstructions from the channels in the graphite plates (as in Figure 22), also ensuring that the lines between the channels and the gas hose inlets are cleared.
10. Prepare a new MEA by removing it from the packaging, and carefully punching holes in the yellow liner to correspond with the dowel holes in the plates. This can be done with a die punch or a knife.
11. Similarly prepare a pair of gaskets to protect the MEA from being crushed when the bolts are tightened around the cell. One gasket should be used for each gas diffusion layer incorporated

in to the MEA. If an internal reforming layer configuration is used, this adds another GDL to that side of the apparatus, so another gasket must be placed on that side.

12. Place the MEA and gaskets on the plates ensuring that the cathode side of the MEA (as marked by a cut in the yellow liner) is on the cathode side of the apparatus.
13. Carefully close the two graphite plates around the MEA so that the dowels line up with the holes in the plates.
14. Retighten the screws in a star pattern.
15. Replace the cell on the insulation, and reattach the thermocouple, feed lines, and waste lines.
16. Plug in the heating elements to the power outlet.
17. Turn the heat control boxes to the desired temperature and proceed with a test.

Appendix C: Supplemental Data

Below are the graphs for the internal reforming layer experiments which illustrate the same trends that were seen in the graphs used in the report. They show the large increase in internal reforming layer performance for the 3M concentrations.

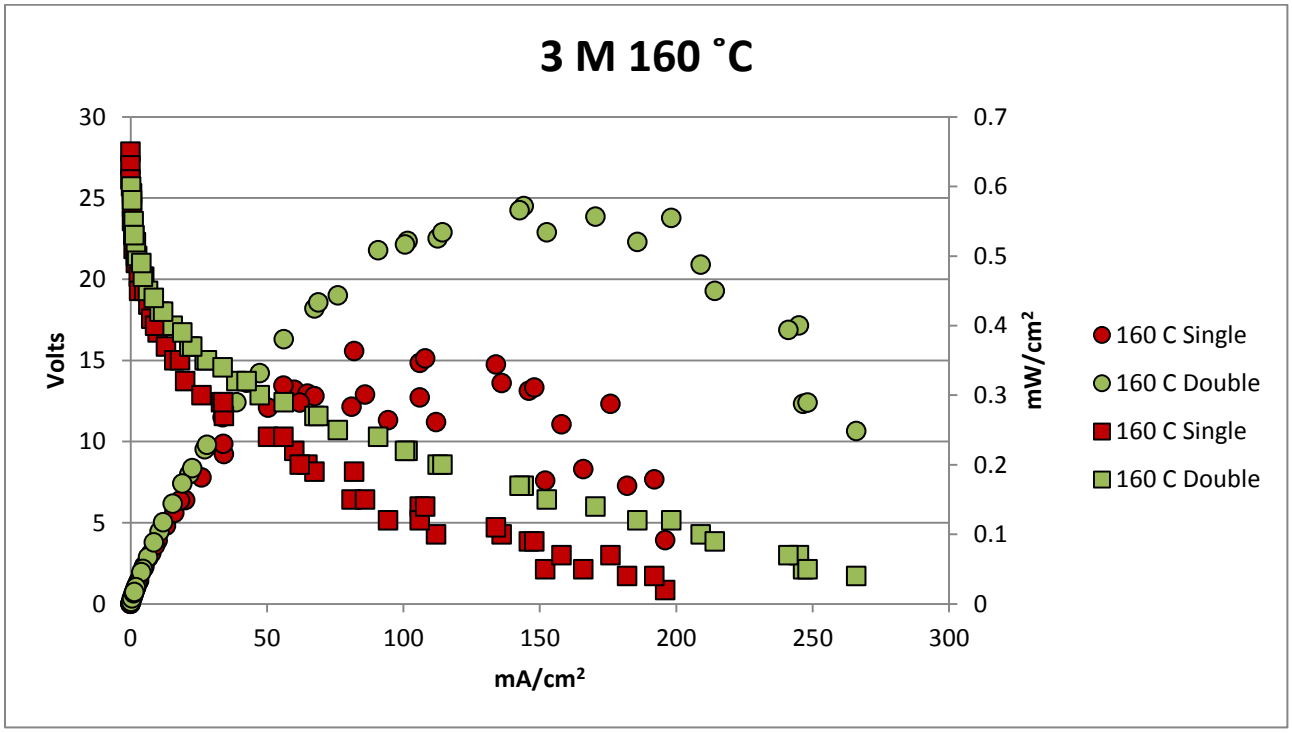

FIGURE 46: 3M INTERNAL REFORMING LAYER 160˚C

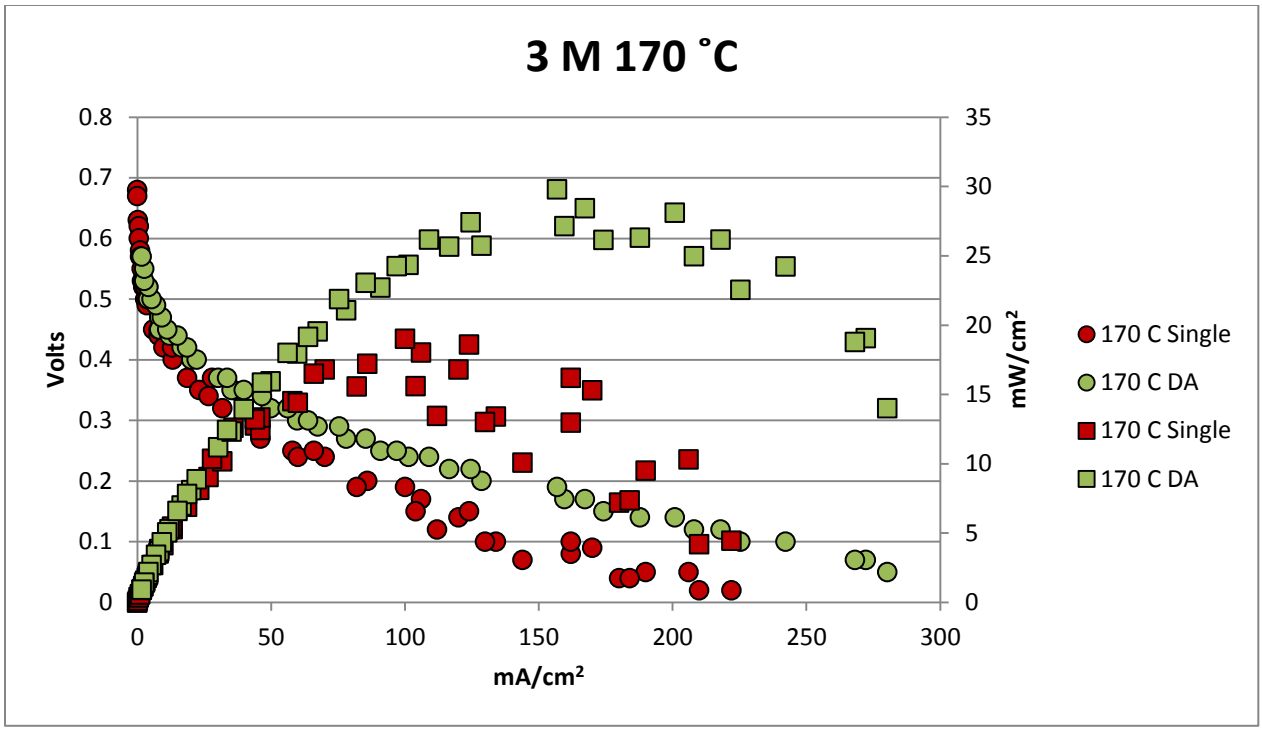

FIGURE 47: 3 M INTERNAL REFORMING LAYER 170˚C

The 5 M concentration internal reforming layer graphs for 160 and 170 degrees Celsius are shown in figures 48 and 49. As in the case of the 10 M concentration mentioned in the report, it appears that 5 M also increases to match the internal reforming layer and single anode tests as temperature increases. This was illustrated more fully through the 10 M single and internal reforming layer tests as they showed a larger gap being closed.

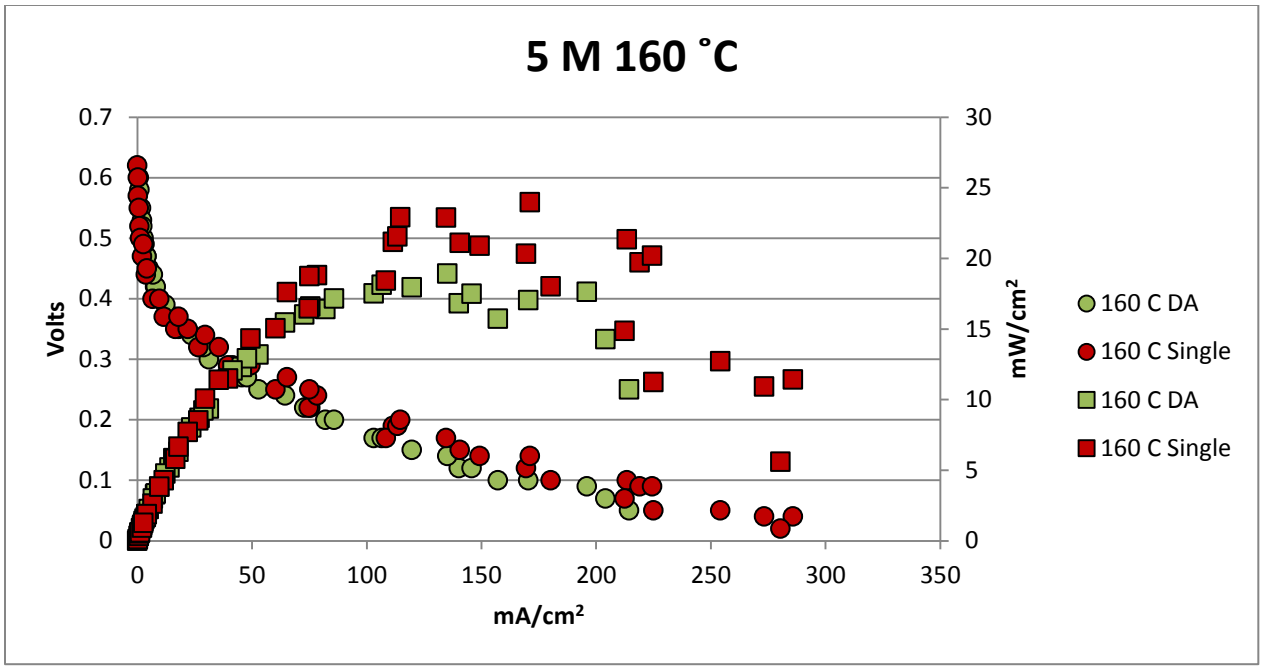

FIGURE 48: 5 M INTERNAL REFORMING LAYER 160˚C

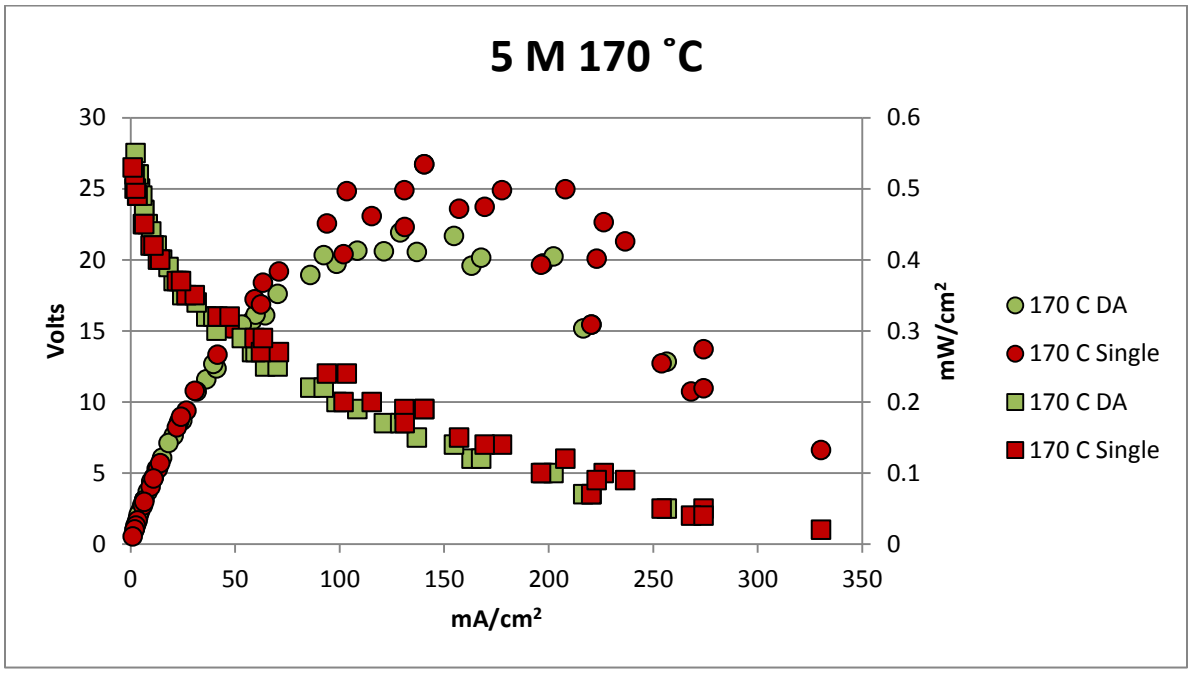

FIGURE 49: 5 M INTERNAL REFORMING LAYER 170˚C